A new in vivo MRI method to non-invasively monitor and quantify the perfusion capacity of 3D-biomaterials grown on the chorioallantoic membrane of chick embryos

Kivrak-Pfiffner, Fatma ; Waschkies, Conny ; Tian, Yinghua ; Woloszyk, Anna ; Calcagni, Maurizio ; Giovanoli, Pietro ; Rudin, Markus ; Buschmann, Johanna

Abstract: Adequate vascularization in biomaterials is essential for tissue regeneration and repair. Current models do not allow easy analysis of vascularization of implants in vivo, leaving it a highly desirable goal. A tool that allows to monitor the perfusion capacity of such biomaterials non-invasively in a cheap, efficient and reliable in vivo model would hence add great benefit to the research in this field. We established, for the first time, an in vivo Magnetic Resonance Imaging (MRI) method to quantify the perfusion capacity of a model biomaterial, DegraPol® foam scaffold, placed on the embryonic avian chorioallantoic membrane (CAM) in ovo. Perfusion capacity was assessed through changes in the longitudinal relaxation rate before and after injection of a paramagnetic MRI contrast agent, Gd-DOTA (®Dotarem, Guerbet S.A.). Relaxation rate changes were compared in three different regions of the scaffold, i.e. at the interface to the CAM, in the middle and on the surface of the scaffold ($p < 0.05$). The highest relaxation rate changes, and hence perfusion capacities, were measured in the interface region where the scaffold was attached to the CAM, whereas the surface of the scaffold showed the lowest relaxation rate changes. A strong positive correlation was obtained between relaxation rate changes and histologically determined vessel density ($R2 = 0.983$), which corroborates our MRI findings. As a proof-of-principle, we measured the perfusion capacity in different scaffold materials, silk fibroin either with or without human dental pulp stem cells. For these, 3 - 4 times larger perfusion capacities were obtained compared to DegraPol®; demonstrating that our method is sensitive to reveal such differences. In summary, we present a novel in vivo method for analyzing the perfusion capacity in 3D- biomaterials grown on the CAM, enabling the determination of the perfusion capacity of a large variety of bioengineered materials.

DOI: https://doi.org/10.1089/ten.TEC.2014.0212

A new *in vivo* MRI method to non-invasively monitor and quantify the perfusion capacity of 3D-biomaterials grown on the chorioallantoic membrane of chick embryos

Fatma Kivrak Pfiffner[1≠], Conny Waschkies, PhD[2,3≠], Yinghua Tian, PhD[3], Anna Woloszyk[4,5], Maurizio Calcagni, MD[1], Pietro Giovanoli, MD[1], Markus Rudin, PhD[2] and Johanna Buschmann, PhD[1*]

≠ These authors contributed equally to the work.

[1]Plastic Surgery and Hand Surgery, University Hospital Zurich, Sternwartstr. 14, 8091 Zurich, Switzerland

[2]Institute for Biomedical Engineering, ETH and University of Zurich, HIT E22.3 Wolfgang-Pauli-Str. 27, 8093 Zurich, Switzerland

[3]Visceral and Transplant Surgery, University Hospital Zurich, Sternwartstr. 14, 8091 Zurich, Switzerland

[4]Institute of Oral Biology, University of Zurich, Schönleinstr. 2, 8091 Zurich

[5]Molecular Life Sciences, University of Zurich and ETH Zurich

*corresponding author: johanna.buschmann@usz.ch

Dr. Johanna Buschmann

University Hospital Zurich

Plastic Surgery and Hand Surgery

Sternwartstrasse 14

8091 Zürich

Word count: 295 (abstract); 3956 (main text); 6 figures, no tables; supporting information: 1 figure

This work was performed at University Hospital Zurich, 8091 Zurich, Switzerland.

Revised version submitted to

Tissue Engineering Part C

August 22, 2014

Addresses of all authors

Fatma Kivrak Pfiffner Kivrak@hotmail.com

Phone +41 44 255 24 79

Fax +41 44 255 50 46

Master of Science in Biology, Plastic Surgery and Hand Surgery, University Hospital Zurich, Sternwartstr. 14, 8091 Zurich, Switzerland

Conny Waschkies Waschkies@biomed.ee.ethz.ch

Phone +41 44 633 76 64

Fax +41 44 633 15 76

PhD, Institute for Biomedical Engineering, ETH and University of Zurich, HIT E22.3 Wolfgang-Pauli-Str. 27, 8093 Zurich, Switzerland

Yinghua Tian Yinghua.tian@usz.ch

Phone +41 44 255 11 11

Fax +41 44 255 44 49

PhD, Visceral and Transplant Surgery, University Hospital Zurich, Sternwartstr. 14, 8091 Zurich, Switzerland

Anna Woloszyk Anna.Woloszyk@zzm.uzh.ch

Phone +41 44 634 31 49

Fax +41 44 634 43 10

PhD student, Institute of Oral Biology, University of Zurich, and Molecular Life Sciences, University of Zurich and ETH Zurich

Maurizio Calcagni Maurizio.calcagni@usz.ch

Phone +41 44 255 35 40

Fax +41 44 255 50 46

MD, Plastic Surgery and Hand Surgery, University Hospital Zurich, Sternwartstr. 14, 8091 Zurich, Switzerland

Pietro Giovanoli Pietro.giovanoli@usz.ch

Phone +41 44 255 33 39

Fax +41 44 255 44 25

MD, Prof., Plastic Surgery and Hand Surgery, University Hospital Zurich, Sternwartstr. 14, 8091 Zurich, Switzerland

Markus Rudin Rudin@biomed.ee.ethz.ch

Phone +41 44 633 76 04

Fax +41 44 633 11 87

PhD, Prof., Institute for Biomedical Engineering, ETH and University of Zurich, HIT E22.4 Wolfgang-Pauli-Str. 27, 8093 Zurich, Switzerland

Johanna Buschmann Johanna.buschmann@usz.ch

Phone +41 44 255 98 95

Fax +41 44 255 50 46

PhD, Plastic Surgery and Hand Surgery, University Hospital Zurich, Sternwartstr. 14, 8091 Zurich, Switzerland

Tissue Engineering Part C: Methods

Abstract

Adequate vascularization in biomaterials is essential for tissue regeneration and repair. Current models do not allow easy analysis of vascularization of implants *in vivo*, leaving it a highly desirable goal. A tool that allows to monitor the perfusion capacity of such biomaterials non-invasively in a cheap, efficient and reliable *in vivo* model would hence add great benefit to the research in this field.

We established, for the first time, an *in vivo* Magnetic Resonance Imaging (MRI) method to quantify the perfusion capacity of a model biomaterial, DegraPol® foam scaffold, placed on the embryonic avian chorioallantoic membrane (CAM) *in ovo*. Perfusion capacity was assessed through changes in the longitudinal relaxation rate before and after injection of a paramagnetic MRI contrast agent, Gd-DOTA (®Dotarem, Guerbet S.A.). Relaxation rate changes were compared in three different regions of the scaffold, i.e. at the interface to the CAM, in the middle and on the surface of the scaffold ($p < 0.05$). The highest relaxation rate changes, and hence perfusion capacities, were measured in the interface region where the scaffold was attached to the CAM, whereas the surface of the scaffold showed the lowest relaxation rate changes. A strong positive correlation was obtained between relaxation rate changes and histologically determined vessel density ($R^2 = 0.983$), which corroborates our MRI findings. As a proof-of-principle, we measured the perfusion capacity in different scaffold materials, silk fibroin either with or without human dental pulp stem cells. For these, 3 – 4 times larger perfusion capacities were obtained compared to DegraPol®; demonstrating that our method is sensitive to reveal such differences.

In summary, we present a novel *in vivo* method for analyzing the perfusion capacity in 3D-biomaterials grown on the CAM, enabling the determination of the perfusion capacity of a large variety of bioengineered materials.

Key words

Chorioallantoic membrane (CAM), DegraPol®, perfusion capacity, vascularization, magnetic resonance imaging (MRI)

Introduction

Tissue engineered constructs for regenerative medicine are based on scaffolds that are used as a matrix for cells to attach and proliferate, so that these artificial grafts can be implanted at defect sites. For this purpose they should provide a high level of biocompatibility. Moreover, vascularization is often required, i.e. the grafts should be easily vascularized after implantation and guarantee long-term functionality and survival of the implanted material and cells. To sustain the artificial graft in an environment as a functional tissue, it is necessary that the blood vessels penetrate the porous grafts from the surrounding tissue since the transport of oxygen and nutrients is dependent on a homogenously distributed vascular network in the implanted scaffold (1-5).

Artificial engineered grafts can have different effects on vascularization. Not only the pore size, but also the size of the scaffold and the interconnectivity of the pores are important criteria for blood-vessel ingrowth after implantation (3, 4). Numerous *ex vivo* and *in vivo* approaches have been established in order to monitor vascularization of tissue grafts including rodents, chicken and fish (6, 7) . *Ex vivo* assays are rapid but more limited because of the lack of inflammation and metabolic processes that may affect the vascularization. Most of the currently available *in vivo* assays involve time, money, and repetitive animal sacrifice, and they are complex and sometimes not easy to compare (3, 8). The chorioallantoic membrane (CAM) of the chick embryo is a well-established model for studying vascularization *in vitro* and *in vivo* and is typically referred to as CAM assay (9, 10). It is a very useful model because of the easy accessibility of the vascular network. Moreover, its lack of immune competence enables studies dealing with tumor growth, wound healing, angiogenesis, anti-angiogenesis or biocompatibility of xenografts (3, 11, 12). In addition, the CAM provides an excellent environment where the cells can attach and proliferate in 3D scaffolds. Finally, the CAM assay is a rapid, simple and low-cost screening method for tissue reactions towards biomaterials (9).

An increasing amount of literature highlights the as yet unmet need to non-invasively monitor the vascularization extent of the implanted scaffolds in order to analyze the success of tissue

regeneration *in vivo* (13, 14). To date, there are only few studies which use Magnetic Resonance Imaging (MRI) as a non-destructive, non-invasive method to study biomaterials on the CAM (9, 10). Our current work presents for the first time the application of MRI to measure the perfusion capacity of CAM-implanted scaffolds *in situ* on the CAM in the living chicken embryo. This method allows a continuous, longitudinal monitoring of developing vessels and hence perfusion capacity in biomaterials *in vivo*.

The particular objectives of our study were (i) to quantify the perfusion capacity within a model scaffold biomaterial, DegraPol® foam, implanted for 7 days on the CAM by MRI *in ovo* and *in vivo* as a function of local distance from the CAM and as a function of time after contrast agent injection,(ii) to correlate our MRI findings with histological analyses of vessel density, and (iii) to apply the established method as a proof-of-principle to different biomaterials discovering the impact of human dental pulp stem cells (hDPSCs) on the perfusion capacity of a silk fibroin scaffold. In sum, we present a new and low cost screening method to study angiogenesis-related questions in the field of tissue-engineered biomaterials.

Materials and Methods

Scaffolds

DegraPol®: The synthetic polyester-urethane DegraPol® is a biocompatible and biodegradable material based on poly-hydroxy-butyrate as a crystalline segment and ε-caprolactone as a soft segment (15). Originally, its synthesis aimed at generating a suitable scaffold material for bone tissue engineering (16), but has recently also been shown to be a beneficial scaffold material for cartilage (17), nerves (18) and tendons (19).

DegraPol® foams were kindly provided by *ab medica*, Italy. They were soaked in cyclohexane (Fluka, puriss.) and frozen at -20°C overnight. They were cut into equal pieces of 8 x 4 x 3 mm^3 immediately after removal from the freezer and were dried at room temperature (evaporation of cyclohexane). All foams were sterilized with ethylenoxide before placing them carefully on the chorioallantoic membrane.

Silk fibroin: Silk fibroin is a biocompatible (after the removal of sericin) and biodegradable material whose physical and mechanical properties can be easily manipulated through structural readjustments(20, 21). It is derived from silkworm cocoons of *Bombyx mori*, which contains at least two major fibroin proteins, light and heavy chains, 25 and 325 kDa, respectively(22). Due to its versatility it has become a popular biomaterial for various applications, e.g. in bone tissue engineering(20). Silk fibroin scaffolds (Trudel Silk Inc., Zurich, Switzerland) with a diameter of 5 mm, a height of 3 mm and a pore size of 200 – 300 µm were used. They were prewetted for 36 h in phosphate buffered solution to rehydrate them before use. After autoclaving (121 °C, 1 bar, 20 min) scaffolds were immersed either in a cell-suspension (0.5 x 10^6 cells/ scaffold) or in cell-free culture medium, respectively. As culture medium, DMEM/F12 (Sigma, D8437) with 10 % FBS (PAN Biotech GmbH, 2602-P291705), 1 % Pen/Strep (Sigma, P0781), 1 % L-Glutamine (Sigma, G7513) and 0.02 % fungizone (Invitrogen, 15290-018) was used. Cell-seeded and cell-free scaffolds were placed in the incubator (37 °C, 5 % CO_2) to allow attachment of the cells. After 1 h scaffolds were washed in fresh

culture medium and placed into a 24-well-plate with 0.8 mL of culture medium in the incubator overnight. After that the scaffolds were placed on the CAM of the fertilized chicken eggs.

Cells

HDPSCs were obtained from dental pulps of healthy teeth of adult patients after the extraction of impacted wisdom teeth. The procedure was approved by the Kantonale Ethikkommission of Zurich (reference number 2012-0588) and performed with written patients' consent. After the removal of the dental pulp from the tooth, hDPSCs were isolated, expanded and characterized as described previously(23).

CAM assay

Fertilized Lowman white LSL chick eggs (Animalco AG Geflügelzucht, Staufen, Switzerland) were incubated at 37°C and 65% relative humidity. On incubation day (ID) 3.5 a circular window with a diameter of 40 - 45 mm was drilled into the eggshell after removing 2 mL albumen so that the developing chorioallantoic membrane detached from the eggshell. The window in the eggshell was closed with a sterile Petri dish of 50 mm to prevent dehydration. On ID 7, DegraPol® foam scaffolds, cell-seeded silk fibroin scaffolds and cell-free silk fibroin scaffolds were carefully placed on top of the chorioallantoic membrane, one scaffold into each egg. The scaffolds were put in the middle of 1 cm-diameter plastic rings to flatten the surface of CAM (Figure 1). Afterwards the eggs were incubated for another 7 days until ID 14.

In vivo assessment of perfusion capacity using MRI

On ID 14, vascularization of the scaffold by capillaries of the chick embryo's chorioallantoic membrane was studied *in situ* on the CAM ("*in ovo*") of the living chicken embryo ("*in vivo")* using Magnetic Resonance Imaging (MRI) in 8 samples. For the MRI examination, the eggs were placed onto a custom-built sliding bed and enveloped by warm water tubing to maintain the temperature of the chick embryo in a physiological range. To prevent motion of the chick embryos, they were

sedated with 5 drops of 1:100 M ketamine (Ketasol-100, Graeub, Switzerland) dripped onto the CAM surface.

MRI was performed with a 4.7 T/16 cm Bruker PharmaScan small animal scanner (Bruker BioSpin, Ettlingen, Germany) equipped with an actively decoupled two-coil system consisting of a 72 mm bird cage resonator for excitation and a 20 mm single loop surface coil for reception. The surface coil was fixed on the Petri dish that covered the eggshell window directly above the scaffold for optimal sensitivity.

Anatomical reference images were obtained in coronal, transversal and sagittal slice orientations (FLASH sequence, TR/TE 200/3 ms, image matrix size 128 x 128, field of view 60 x 60 mm^2, 5 slices, images reconstructed to a nominal resolution of 0.23 x 0.23 x 1 mm^3, total scan time 25 s). T_1-weighted MR images were acquired with a RARE sequence of variable TR and TE for quantitative T_1 and T_2 mapping (TR 200/400/800/1500/3000/4500ms, TE 10/30/50/70/90ms, RARE-factor 2, image matrix size 220 x 150, field of view 45 x 30 mm^2, spatial resolution 0.2 x 0.2 mm^2, slice thickness 1 mm, total scan time 9 min 40 s).

T_1 maps were acquired in 8 DegraPol®, 4 silk fibroin and 4 silk fibroin samples seeded with hDPSCs before and after i.v. injection 100 µL 0.05 M Gd-DOTA MRI contrast agent (Dotarem®, Guerbet S.A., Switzerland). The time between Gd-DOTA injection and T_1 mapping was held constant at 25 min. An additional time series was acquired in 3 DegraPol®samples with T_1 map acquired at 15, 25, 35, 45 and 60 min post-injection.

T_1 relaxation times were determined in three regions of interest at (i) the surface of the scaffold, (ii) in the middle, and (iii) at the interface of the scaffold with the CAM. Perfusion capacity in these three regions of interest was assessed through changes in the longitudinal relaxation rate, $\Delta R_1=R_1-R_{10}$, before and after injection of Gd-DOTA, as the relaxation rate changes with the amount of gadolinium present in the CAM:

$$R_1 = R_{10} + r_1 \cdot [Gd]$$

where

$R_1 = 1/ T_1$

are the longitudinal relaxation rate after and R_{10} before contrast agent administration and r_1 the molar relaxivity of the contrast agent in s^{-1} mol^{-1} L and [Gd] the concentration of Gd in mol L^{-1}.

Intravenous injection of Gd-DOTA

For intravenous injection of the MRI contrast agent, eggs were placed on a 37 °C heating bed and i.v. injection was performed under a surgical microscope with 12 – 20 x magnification. A big and straight vein on the surface was selected and grasped by a microsurgical forceps and 100 µL Gd-DOTA slowly injected with a 1.0 mL syringe and 30G needle. A cotton sticker was placed on the injection site of the vessel with slight pressure before the syringe was withdrawn to prevent bleeding.

Histological analyses

After completion of the MRI measurements the scaffold-CAM complex was fixed overnight using 4 % formalin solution in PBS, then excised, embedded in paraffin, cross-sectioned in 5 µm slices and stained with H&E, CD31 (PECAM-1 (M-20): sc-1506, Santa Cruz Biotechnology; staining procedure for paraffin sections of the VECTASTAIN Elite ABC Kit-Rabbit IgG (PK-6101; VECTOR LABORATORIES, INC., Burlingame, CA, USA)) and *Von Willebrand Faktor* (Factor VIII) (Dako) according to established procedures (24). Slices were obtained from three regions of the scaffold: (i) surface, (ii) middle, and (iii) interface to the CAM, and 3 - 4 slices for each region were analyzed. The vessel density was scored semi-quantitatively by counting the number of vessels manually under a light microscope (Leica DM 6000 B, Zurich, Switzerland) equipped with a digital camera; with **0** = no vessels, **1** = < 10, **1.5**= 10 - 30, **2** = 30 - 50, **2.5** = 50 - 70, **3** = 70 - 90, **3.5** = 90 - 110, **4** = 110 – 130, **4.5** = 130-150 and **5** = > 150 vessels in a cross-section of 32 mm^2.

Statistics

The correlation of capillarity densities and the change in relaxation rates, ΔR_1, was determined by linear regression using StatView 5.0.1. Moreover, one-way analysis of variance (ANOVA) was conducted. Pairwise comparison probabilities (*p*) were calculated using the Fisher's PLSD. P values < 0.05 were considered significant.

Tissue Engineering Part C: Methods

Results

MRI measurements

The ability to quantify the perfusion capacity is crucial for assessing the biocompatibility of tissue-engineered grafts and biomaterials. Here, we used MRI to assess perfusion capacity through changes in the R_1 relaxation rates, ΔR_1, before and after injection of a paramagnetic MRI contrast agent, Gd-DOTA. In **Figure 2**, T_1-weighed images before and after injection are depicted. In the pre-contrast image, the scaffold and supportive plastic ring and head of the chick embryo can be distinguished, but are much better delineated in the post-contrast image, as the scaffold and embryonic structures show high contrast enhancement, while the adjacent tissue shows little uptake. As for the scaffold material implanted on the CAM, it is shown that contrast enhancement varies locally within the scaffold and that the largest signal change appears at the interface to the CAM (see enlarged section that zooms into the scaffold). Noteworthy to mention is the clear border of the contrast agent uptake at the interface to the CAM. While little Gd-DOTA uptake is found next to the scaffold implying little vascularization, there is a high contrast agent uptake at the interface. A quantitative analysis is summarized in **Figure 3**, which shows that the relaxation rate change, ΔR_1, and hence perfusion capacity, declines from interface to the CAM towards the surface region of the scaffold (n = 8).

Finally, the relaxation rate change, ΔR_1, was monitored as a function of time after injection of Gd-DOTA (n = 3). As shown in **Figure 4**, the signal intensity reached a plateau at 35 min in all regions of interest studied.

Histology

Quantification of vessel density was accomplished by counting the number of blood vessels within cross-sections of 8 mm x 4 mm stained by H&E (**Figure 5a**). Vessels were identified as roundish blue structures lining endothelial cells. Representative images for each score level are available as supplementary material to this paper (**Supplementary Information SI Figure 1**). Vessel counts from

H&E staining were also confirmed by an additional scoring in *von Willebrand Factor* immunostained corresponding sections (**Figure 5b**). In addition, CD31 staining revealed the same vessel counts as determined by H&E and *von Willebrand Factor* stainings (**Figure 5c**). These histological analyses revealed that the interface region of the implanted DegraPol® scaffold with the CAM showed the highest number of small blood vessels compared to middle and surface, with an average vessel density score of 3.05 ± 1.34; 2.42 ± 1.15 and 1.47 ± 0.65, respectively. The surface region with the longest distance to the CAM had the lowest number of small blood vessels (**Figure 6**). Therefore, the same regional pattern of vascularization was observed as in our MRI data. Furthermore, a strong correlation was obtained between relaxation rate changes, ΔR_1, and the histological scores for vessel density (R^2= 0.983). Thus, the histology data corroborate the MRI findings.

Perfusion capacity in different biomaterials (Proof-of-principle)

In order to apply the method to other biomaterials than DegraPol®, relaxation rate changes, ΔR_1, of silk fibroin scaffolds (± hDPSCs) were measured for the same corresponding scaffold regions (interface, middle and surface, **Figure 3**). For all three regions, the perfusion capacity of silk fibroin scaffolds was significantly higher compared to the DegraPol® scaffolds (3 - 4 times higher, $p < 0.0001$). However, the hDPSCs did not evoke a statistically significant higher perfusion of the silk fibroin scaffolds compared to the cell-free silk fibroin scaffolds ($p > 0.1$). Only a trend was noticed for all three regions, where the perfusion was higher in the presence of the hDPSCs compared to the cell-free scaffolds. CD31 staining clearly showed the vessels inside the silk fibroin scaffold seeded by hDPSCs (**Figure 5d**). Finally, in both biomaterials, DegraPol® as well as silk fibroin (± hDPSCs), perfusion capacity declines from the interface towards the surface, in line with the scaffolds being vascularized from the CAM towards the surface.

Discussion

In the current study, we present for the first time a cheap screening method for non-invasive quantification of the perfusion capacity of biomaterials with MRI *in vivo.* We found a strong positive correlation between local changes in T_1- based relaxation rates in biomaterials grown 1 week on the chorioallantoic membrane (CAM) and the vessel density determined by histology.

Vascularization in three-dimensional biomaterials is a limiting factor for successful implantation and functionalization of these engineered tissues. The highly vascularized CAM of the chick embryo is a useful model to evaluate the tissue response and perfusion capacity of scaffolds placed on top of the CAM. Furthermore, this avian model provides a good nutritional environment to tissue-engineered materials. Compared to the traditional mammalian models, the CAM assay is cheap, more time efficient and does not have any immune-system based reaction towards foreign bodies (6). Thus, it allows – among many other applications - to work with human tumor cells in order to study tumor-induced angiogenesis (25) or chemoprevention (26). Even in environmental pollution and health debates, it may serve as a valuable model (27). Finally, the CAM assay has been well established (6), is low priced and predominantly used to study angiogenesis and anti-angiogenesis in response to different drugs, growth factors and cell types (3, 28).

As a model biomaterial, we chose a biodegradable DegraPol® foam because this polyester-urethane has been shown to be biocompatible with respect to osteoblasts (16), chondrocytes (17) and tenocytes(29) among others. To date, many studies examined the tissue response towards biomaterials using the CAM model (3, 8), or tested different biomaterials such as PVC or modified polyurethanes with respect to angiogenesis and inflammatory response (30).However, they often use “end-point” information such as histological analysis which necessitates the destruction of the tissue-engineered construct. In a previous study we therefore presented MRI as a non-destructive, analytical tool for studying vascularization *ex vivo* in the same biomaterial grown on the CAM (10). While MRI has been employed *in vivo* to determine the mineralization of bone constructs placed on

the CAM (9), it has not been used so far for the assessment of the perfusion capacity. Our present study therefore shows for the first time MRI as a suitable method to examine the perfusion capacity in biomaterials placed on the CAM *in situ in the living chicken embryo.* The combination of the CAM model with an *in ovo* and *in vivo* MRI readout offers the potential to longitudinally monitor the perfusion capacity of biomaterials. In other words, the vascularization process can be followed *in vivo* by non-invasive MRI, thereby offering a novel screening method to quantify the perfusion capacity of a series of different biomaterials at different time points in the same sample.

In particular, our data show that the perfusion capacity of scaffolds grown for one week on the CAM can be quantified by analyzing relaxation rate changes, as these are dependent on the amount of contrast agent present in the vascular network. Inspection of contrast-enhancement within the scaffold revealed regional variations and a region of interest analysis of relaxation rate changes was performed to assess such heterogeneity more quantitatively. As such, perfusion capacity was found to be highest at the interface where the scaffold was attached to the CAM while it gradually decreased with distance from the interface with lowest perfusion capacity found at the surface of the scaffold. Presumably, DegraPol® scaffolds were too large to be fully vascularized as has been found for smaller DegraPol® foams (30 mm^3 as compared to 96 mm^3 used here) in our previous study (10). Semi-quantitative histological analyses of vessel density in locally staggered histological sections taken from the interface, middle and surface of the scaffold corroborates the MRI findings as the highest vessel density was found at the interface and lowest at the surface of the scaffold. Furthermore, histological scores were found to strongly correlate with the relaxation rate changes, providing further support for our notion that relaxation rate changes may be used as a simplified measure for perfusion capacity.

In order to apply this newly established method to a typical question in the field of tissue engineering (as a proof-of-principle), silk fibroin scaffolds either with or without hDPSCs were also analyzed with respect to their perfusion capacity by MRI. First of all, the differences in the relaxation rates between the two materials DegraPol® and silk fibroin were significant; silk fibroin showed 3 - 4 times higher

relaxation rates compared to DegraPol®, which renders silk fibroin a much better scaffold material in terms of a fast vascularization. Secondly, silk fibroin seeded with hDPSCs had higher relaxation rates compared to cell-free constructs (trend), implying that an *in vitro* preseeding of only one day (!) has already a beneficial impact on the perfusion extent *in ovo*. The hDPSCs are involved in the building of new vessels inside the silk fibroin as confirmed by histological analysis of typical endothelial cell markers (von Willebrand Factor and CD31). Therefore, our method leads to remarkable changes in ΔR_1 for different scaffold materials as well as it is sensitive already for minor changes in preparation such as a 1-day preseeding by stem cells.

Some limitations of the *in ovo* CAM model as used in our study should be mentioned, however. First, only 30 – 40 % of the windowed eggs survived the opening of the eggshell. This may mostly be attributed to eggshell dust contaminating the otherwise sterile egg cavity and its environment during windowing. Smaller windows might reduce the risk of contamination, however, larger windows allow minimizing the distance between the scaffold and the surface coil during MRI measurements and facilitate access to the vasculature during contrast agent injection, which is necessary for higher resolutions. Second, the injection of the contrast agent was a highly delicate process due to the small vessel size and flexibility within the egg yolk. An experienced microsurgeon (Y.T.) provided the required skills, but these can be also acquired by others through dedicated trainingThird, there is a limitation in size of the biomaterial under investigation; a size of 8 x 4 x 3 mm^3 as used in case of the DegraPol® scaffolds could have a bigger area placed on the CAM, however, the height (3 mm) cannot be increased much because during a time frame of 7 days, vessel growth starting from the CAM surface might not reach the top of the scaffold. Moreover, the timing between contrast agent injection and relaxation time measurement was set at 25 min. This time window was considered ample for the contrast agent to distribute in the microvasculature and extravascular compartment and the relaxation rate change, and hence perfusion signal, being not dominated by wash-in effects of bigger vessels. In order to assess possible effects of this specific time window we acquired a time series of relaxation rate changes between 15 - 60 min post-injection in 3 samples. These data reveal

that contrast agent uptake is highest 35 min post-injection, indicating that other processes, such as diffusion, also contribute to the rather slow contrast agent uptake (31). Thus, for highest contrast our preset time window of 25 min post-injection, which was preset such as to maximize uptake of contrast agent but also aimed at reducing necessary scantime, will be increased in future studies.

Finally it should be mentioned that in our study we did not take full advantage of our method's potential to perform longitudinal measurements that our *in ovo* CAM model combined with non-invasive *in vivo* MRI readout offers. In order to do so, a couple of legal, physiological and technical issues will need to be tackled: Experimental procedures with fertilized eggs fall under the legislation of the Swiss federal ordinance on animal protection and welfare starting on ID 14 and hence the prerequisite legal framework needs to be set into place for experiments lasting longer than ID 14. On the physiological side it remains to be established how much the development of the vascular network and ultimately perfusion capacity is affected by stress induced by the handling of the egg, anesthesia, MRI measurement and contrast agent injection. Previous studies indicate that such effects exist and warrant further investigation (32). And finally, contrast agent doses might need to be titrated down such as to enable repeated measurements, in particular as renal clearing rates in the avian embryo are not known and the contrast agent supposedly remains in the closed environment of the egg.

Nevertheless, the method established here is really beneficial for tissue engineering and regeneration purposes because it allows performing a cheap and fast *in vivo* screening of the perfusion extent of any biomaterials or bio-artificial constructs. It hence allows gathering valuable preclinical information about a material's potential long-term functionality and survival in the host tissue and therefore may steer early candidate selection for further development. Furthermore, for the benefit of the 3 R's, it has become mandatory to evaluate cell-scaffold constructs prior to *in vivo* experiments (33). With a cost of only 2 dollars per egg it is much cheaper compared to animal models such as mice (> 25 dollars), rats (> 35 dollars) or rabbits (> 200 dollars). Moreover, vascularization of the biomaterials can be monitored as a function of time with non- invasive MRI and valuable

information can be gathered within a time frame of only two weeks including one week of incubation and one week of monitoring angiogenesis in the material under view.

In sum, the CAM model's cost effectiveness and the absence of immune-defense reactions combined with the non-invasiveness of MRI to access the perfusion capacity of biomaterials and tissue engineered constructs *in vivo* and *in ovo* will increase the attractiveness of this distinguished combination in the future. We conclude that the CAM assay together with non-invasive MRI presents a reliable *in vivo* model for monitoring the perfusion capacity of biomaterials. Further studies are planned with arrays of different biomaterials and differently pre-engineered biomaterials in our laboratory.

Acknowledgements

We would like to thank Ms. Pia Fuchs for H&E staining and Dr. Monika Hilbe for *von Willebrand Factor* staining. PD Dr. Andreas Boss is acknowledged for providing the contrast agent. Furthermore, Trudel Silk Inc., Zurich, Switzerland is highly acknowledged for providing silk fibroin and Dr. Sandra Hofmann, Eindhoven University of Technology, for manufacturing the scaffolds. We additionally thank PD Dr. Dr. Bernd Stadlinger of the clinic for dental medicine, for providing the theeth. The Matching Funds of University Hospital Zurich are highly acknowledged for financial support. We are thankful to *ab medica,* Italy, for providing the DegraPol® foams.

Author Disclosure Statement

There are no competing financial interests of all authors.

References

1. Lemon, G., Howard, D., Tomlinson, M.J., Buttery, L.D., Rose, F.R.A.J., Waters, S.L., King, J.R. Mathematical modelling of tissue-engineered angiogenesis. Mathematical Biosciences **221**, 101-20, 2009.
2. Borges, J., Tegtmeier, F.T., Padron, N.T., Mueller, M.C., Lang, E.M., Stark, G.B. Chorioallantoic membrane angiogenesis model for tissue engineering: A new twist on a classic model. Tissue Eng **9**, 441-50, 2003.
3. Baiguera, S., Macchiarini, P., Ribatti, D. Chorioallantoic membrane for in vivo investigation of tissue-engineered construct biocompatibility. J Biomed Mater Res Part B **100B**, 1425-34, 2012.
4. Rouwkema, J., Rivron, N.C., van Blitterswijk, C.A. Vascularization in tissue engineering. Trends Biotechnol **26**, 434-41, 2008.
5. O'Brien, F.J. Biomaterials & scaffolds for tissue engineering. Mater Today **14**, 88-95, 2011.
6. Deryugina, E.I., Quigley, J.P. Chick embryo chorioallantoic membrane models to quantify angiogenesis indued by inflammatory and tumor cells or purified effector molecules. Methods in Enzymology2008. pp. 21-41.
7. Cole, R.W., Liu, F., Herron, B.J. Imaging of angiogenesis: past, present and future. Microscopy: Science, Technology, Applications and Education **1**, 885-96, 2010.
8. Valdes, T.I., Kreutzer, D., Moussy, F. The chick chorioallantoic membrane as a novel in vivo model for the testing of biomaterials. J Biomed Mater Res **62**, 273-82, 2002.
9. Chesnick, I.E., Fowler, C.B., Mason, J.T., Potter, K. Novel mineral contrast agent for magnetic resonance studies of bone implants grown on a chick chorioallantoic membrane. Magn Reson Imaging **29**, 1244-54, 2011.
10. Buschmann, J., Welti, M., Hemmi, S., Neuenschwander, P., Baltes, C., Rudin, M., Giovanoli, P., Calcagni, M. 3D co-cultures of osteoblasts and endothelial cells in DegraPol foam: Histological and high field MRI analyses of pre-engineered capillary networks in bone grafts. Tissue Eng Part A **17**, 291-9, 2011.
11. Klueh, U., Dorsky, D.I., Moussy, F., Kreutzer, D.L. Ex ova chick chorioallantoic membrane as a novel model for evaluation of tissue responses to biomaterials and implants. J Biomed Mater Res Part A **67A**, 838-43, 2003.
12. Lokman, N.A., Elder, A.S.F., Ricciardelli, C., Oehler, M.K. Chick Chorioallantoic Membrane (CAM) Assay as an In Vivo Model to Study the Effect of Newly Identified Molecules on Ovarian Cancer Invasion and Metastasis. Int J Mol Sci **13**, 9959-70, 2012.
13. Krishnan, R., Arora, R.P., Alexander, M., White, S.M., Lamb, M.W., Foster, C.E., Choi, B., Lakey, J.R. Noninvasive evaluation of the vascular response to transplantation of alginate encapsulated islets using the dorsal skin-fold model. Biomaterials **35**, 891-8, 2014.
14. Sauerbier, S., Palmowski, M., Vogeler, M., Nagursky, H., Al-Ahmad, A., Fisch, D., Hennig, J., Schmelzeisen, R., Gutwald, R., Fasol, U. Onset and maintenance of angiogenesis in biomaterials: in vivo assessment by dynamic contrast-enhanced MRI. Tissue Eng Part C-Methods **15**, 455-62, 2009.
15. Milleret, V., Simonet, M., Bittermann, A.G., Neuenschwander, P., Hall, H. Cyto- and hemocompatibility of a biodegradable 3D-scaffold material designed for medical applications. J Biomed Mater Res Part B **91B**, 109-21, 2009.
16. Saad, B., Casotti, M., Huber, T., Schmutz, P., Welti, M., Uhlschmid, G.K., Neuenschwander, P., Suter, U.W. In vitro evaluation of the biofunctionality of osteoblasts cultured on DegraPol-foam. J Biomater Sci-Polym Ed **11**, 787-800, 2000.
17. Saad, B., Moro, M., Tun-Kyi, A., Welti, M., Schmutz, P., Uhlschmid, G.K., Neuenschwander, P., Suter, U.W. Chondrocyte-biocompatibility of DegraPol (R)-foam: In vitro evaluations. J Biomater Sci-Polym Ed **10**, 1107-19, 1999.
18. Borkenhagen, M., Stoll, R.C., Neuenschwander, P., Suter, U.W., Aebischer, P. In vivo performance of a new biodegradable polyester urethane system used as a nerve guidance channel. Biomaterials **19**, 2155-65, 1998.

19. Buschmann, J., Meier-Bürgisser, G., Bonavoglia, E., Neuenschwander, P., Milleret, V., Giovanoli, P., Calcagni, M. Cellular response of healing tissue to DegraPol tube implantation in rabbit Achilles tendon rupture repair: an in vivo histomorphometric study. Journal of Tissue Engineering and Regenerative Medicine **7**, 413-20, 2013.

20. Hofmann, S., Hilbe, M., Fajardo, R.J., Hagenmueller, H., Nuss, K., Arras, M., Mueller, R., von Rechenberg, B., Kaplan, D.L., Merkle, H.P., Meinel, L. Remodeling of tissue-engineered bone structures in vivo. European Journal of Pharmaceutics and Biopharmaceutics **85**, 119-29, 2013.

21. Kundu, B., Rajkhowa, R., Kundu, S.C., Wang, X. Silk fibroin biomaterials for tissue regenerations. Advanced Drug Delivery Reviews **65**, 457-70, 2013.

22. Altman, G.H., Diaz, F., Jakuba, C., Calabro, T., Horan, R.L., Chen, J.S., Lu, H., Richmond, J., Kaplan, D.L. Silk-based biomaterials. Biomaterials **24**, 401-16, 2003.

23. Tirino, V., Paino, F., De Rosa, A., Papaccio, G. Identification, Isolation, Characterization, and Banking of Human Dental Pulp Stem Cells. In: Singh SR, ed. Somatic Stem Cells: Humana Press; 2012. pp. 443-63.

24. Ribatti, D., Nico, B., Vacca, A., Roncali, L. Localization of factor VIII-related antigen in the endothelium of the chick embryo chorioallantoic membrane. Histochem Cell Biol **112**, 447-50, 1999.

25. Subauste, M.C., Kupriyanova, T.A., Conn, E.M., Ardi, V.C., Quigley, J.P., Deryugina, E.I. Evaluation of metastatic and angiogenic potentials of human colon carcinoma cells in chick embryo model systems. Clinical & Experimental Metastasis **26**, 1033-47, 2009.

26. Wang, D., Taylor, E.W., Wang, Y., Wan, X., Zhang, J. Encapsulated nanoepigallocatechin-3-gallate and elemental selenium nanoparticles as paradigms for nanochemoprevention. International Journal of Nanomedicine **7**, 1711-21, 2012.

27. Mousa, S.A., O'Connor, L., Rossman, T.G., Block, E. Pro-angiogenesis action of arsenic and its reversal by selenium-derived compounds. Carcinogenesis **28**, 962-7, 2007.

28. Ribatti, D. Chick embryo chorioallantoic membrane as a useful tool to study angiogenesis. International Review of Cell and Molecular Biology, Vol 270. San Diego: Elsevier Academic Press Inc; 2008. pp. 181-224.

29. Sukthankar, A. DegraPol-btc/btgc: In vitro Untersuchung der Biokompatibilität für Tenozyten Surgery Division University Hospital Zurich, University Hospital Zurich, Zurich, 1999.

30. Zwadlo-Klarwasser, G., Gorlitz, K., Hafemann, B., Klee, D., Klosterhalfen, B. The chorioallantoic membrane of the chick embryo as a simple model for the study of the angiogenic and inflammatory response to biomaterials. J Mater Sci-Mater Med **12**, 195-9, 2001.

31. Rudin, M., McSheehy, P.M.J., Allegrini, P.R., Rausch, M., Baumann, D., Becquet, M., Brecht, K., Brueggen, J., Ferretti, S., Schaeffer, F., Schnell, C., Wood, J. PTK787/ZK222584, a tyrosine kinase inhibitor of vascular endothelial growth factor receptor, reduces uptake of the contrast agent GdDOTA by murine orthotopic B16/BL6 melanoma turnours and inhibits their growth in vivo. NMR Biomed **18**, 308-21, 2005.

32. Mohammad, F.K., Faris, G.A.M., Al-Zubeady, A.Z. Developmental and behavioral effects of medetomidine following in ovo injection in chicks. Neurotoxicology and Teratology **34**, 214-8, 2012.

33. Falkner, E., Eder, C., Kapeller, B., Fröschl, W., Schmatz, C., Macfelda, K., Losert, U.M. The mandatory CAM testing of cells and scaffolds for tissue engineering: benefits for the three Rs of cooperation with the vaccine industry. Alternatives to Laboratory Animals **32**, 573-80, 2004.

Tissue Engineering Part C: Methods

Figure Captions

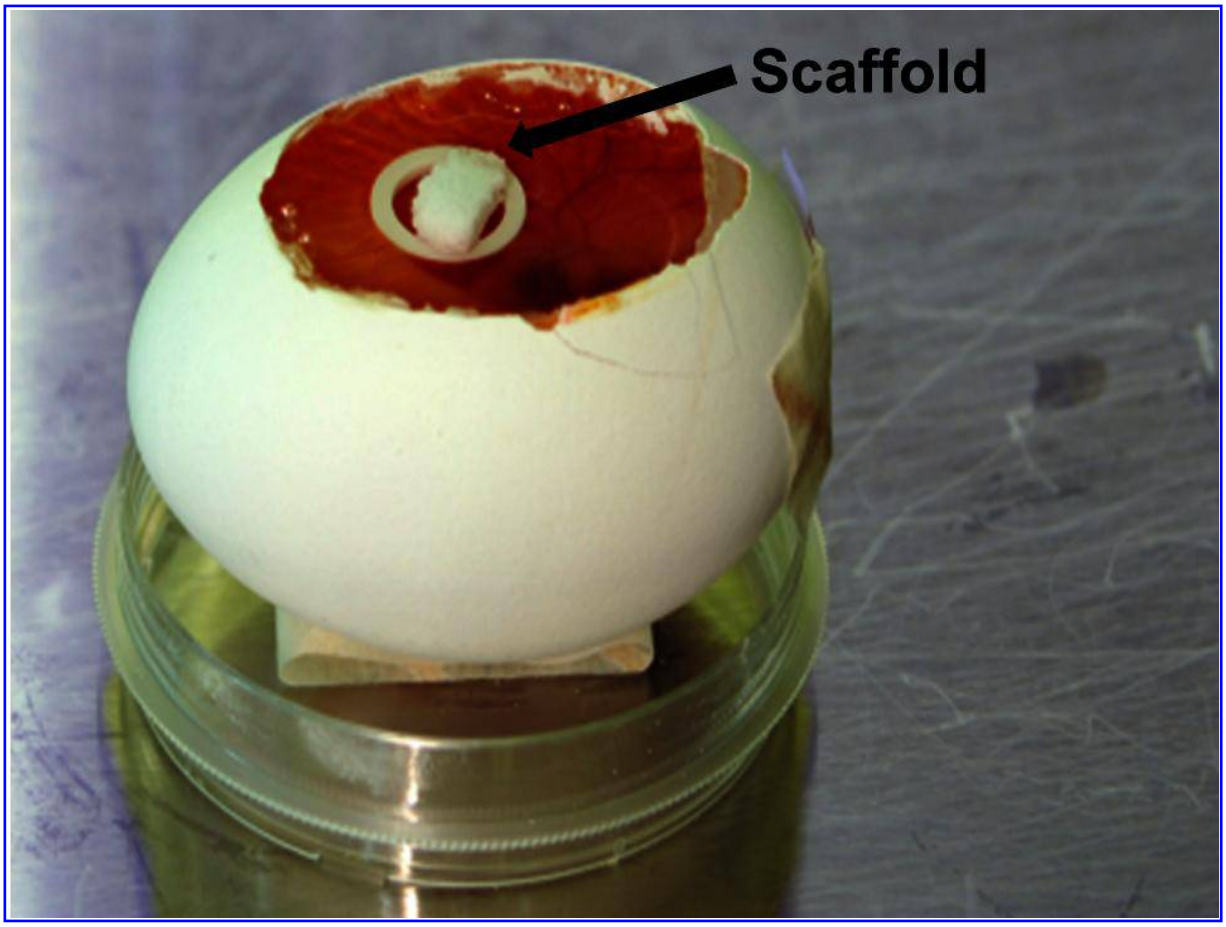

Figure 1. DegraPol® foam scaffold (arrow) placed in the middle of a supportive plastic ring on top of the CAM on ID 7.

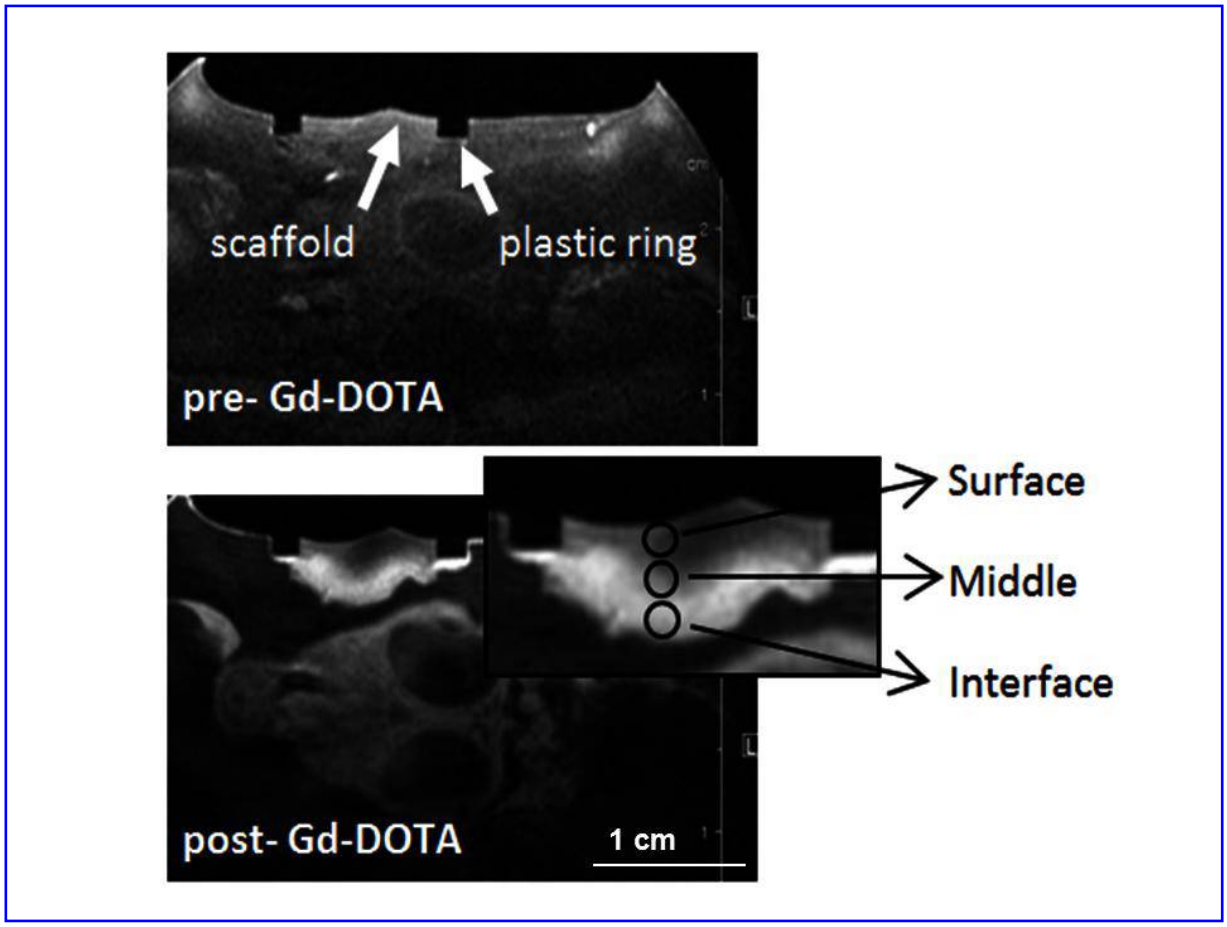

Figure 2. *In ovo* T_1-weighted MRI images acquired 7 days post-implantation in an axial slice through the scaffold. (a) before, (b) 25 min after i.v. injection of Gd-DOTA. Enlarged section: scaffold with regions of interest (circles) at the interface with the CAM, in the middle and on the surface of the scaffold.

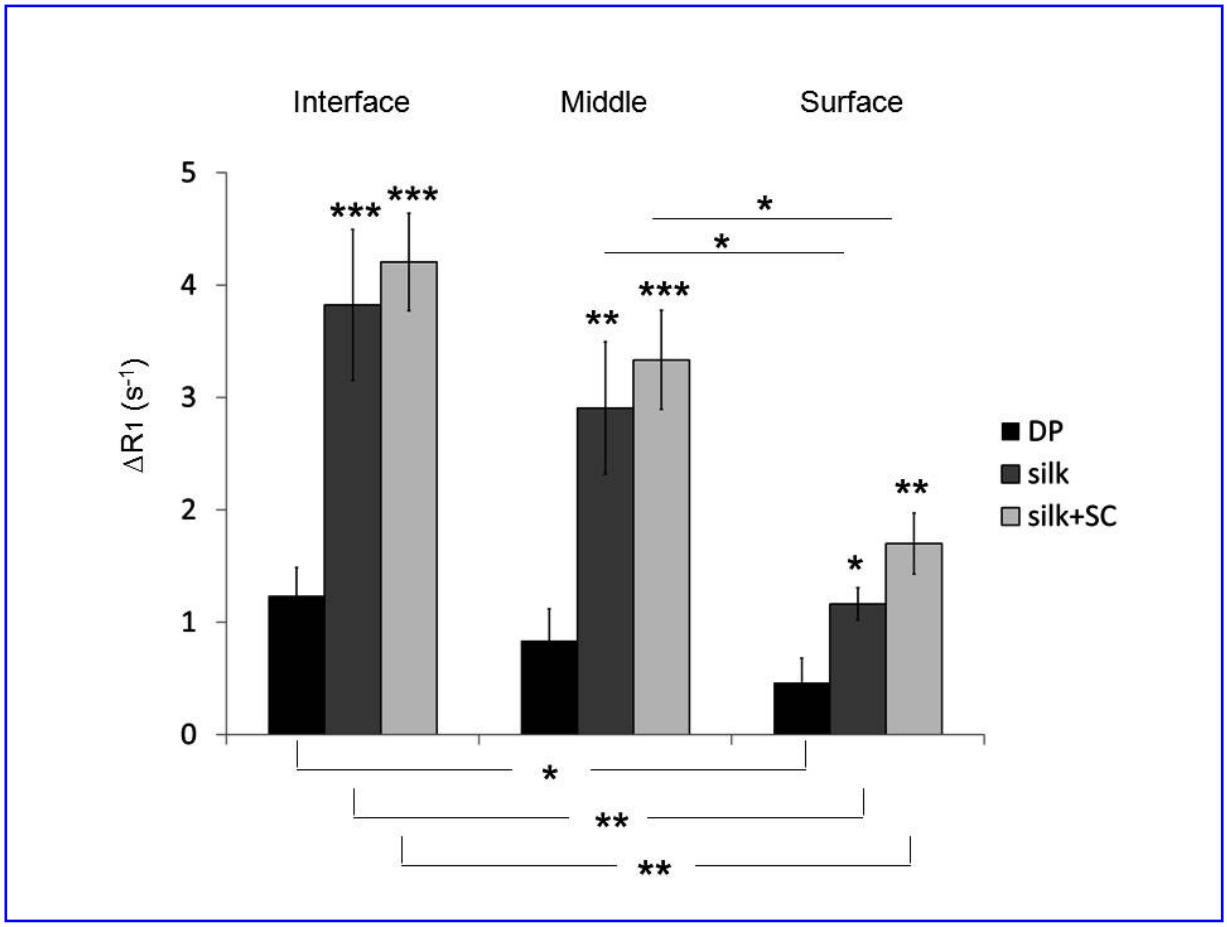

Figure 3. Relaxation rate change ΔR_1 in three regions of interest at the interface, middle and surface of the DegraPol® and silk fibroin scaffolds either with or without human dental pulp stem cells grown for 1 week on the CAM. Values are given as means ± standard deviation. *P*-values are denoted as * is $p < 0.05$; ** $p < 0.01$ and *** $p < 0.001$. Asterisks without line refer to comparisons to DegraPol®.

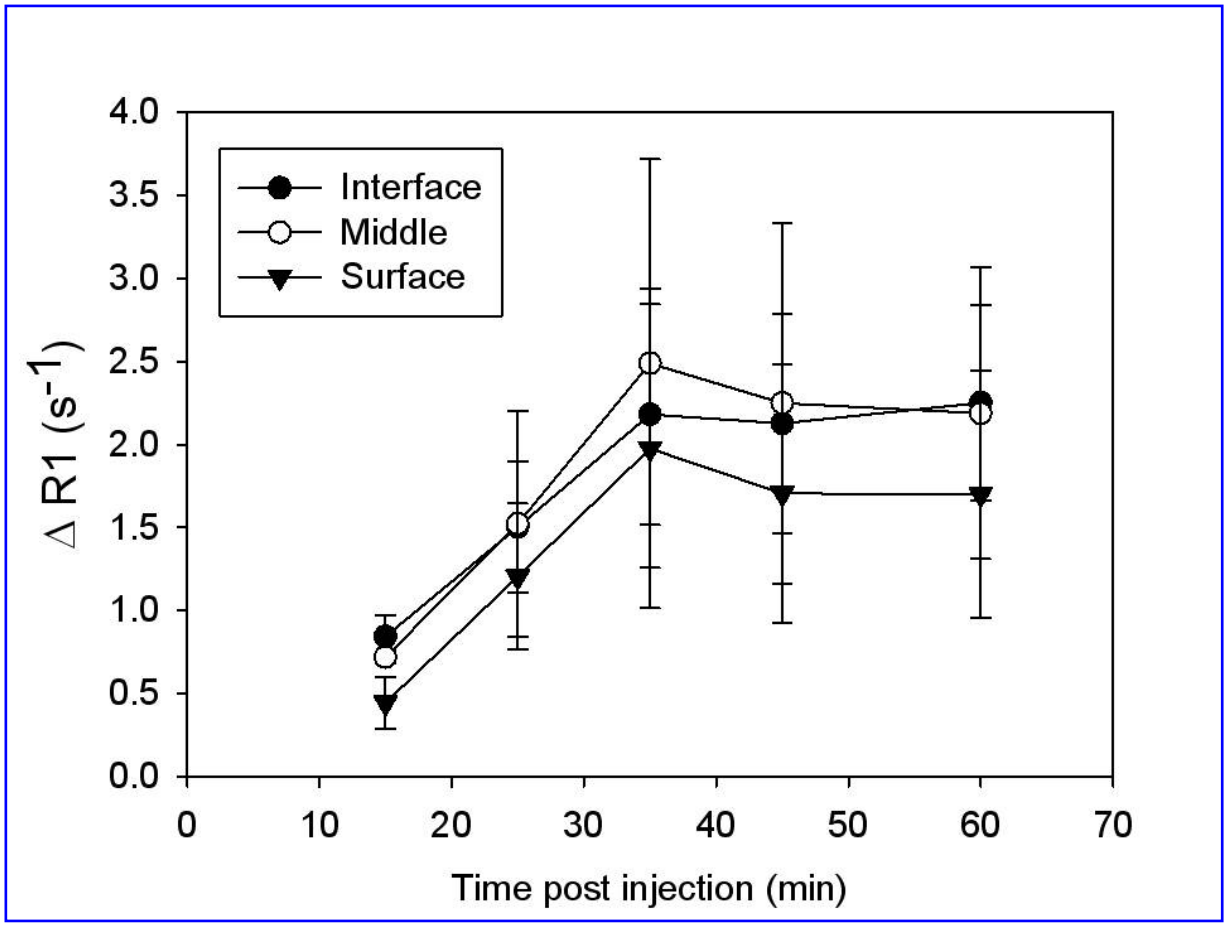

Figure 4. Relaxation rate change ΔR_1 as a function of time after contrast agent injection in three regions of interest at the interface, middle and surface of the DegraPol® scaffold. Values are given as means ± standard deviation.

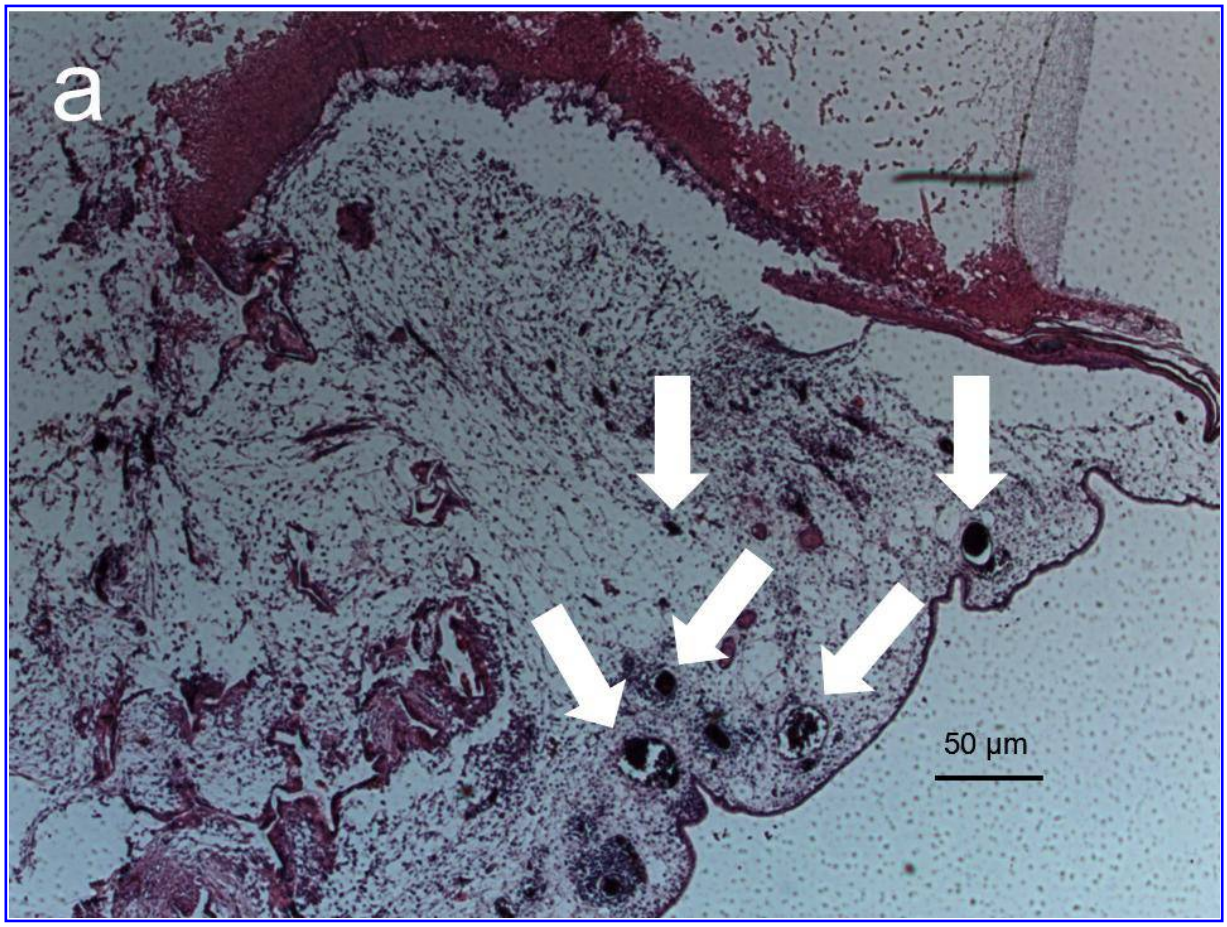

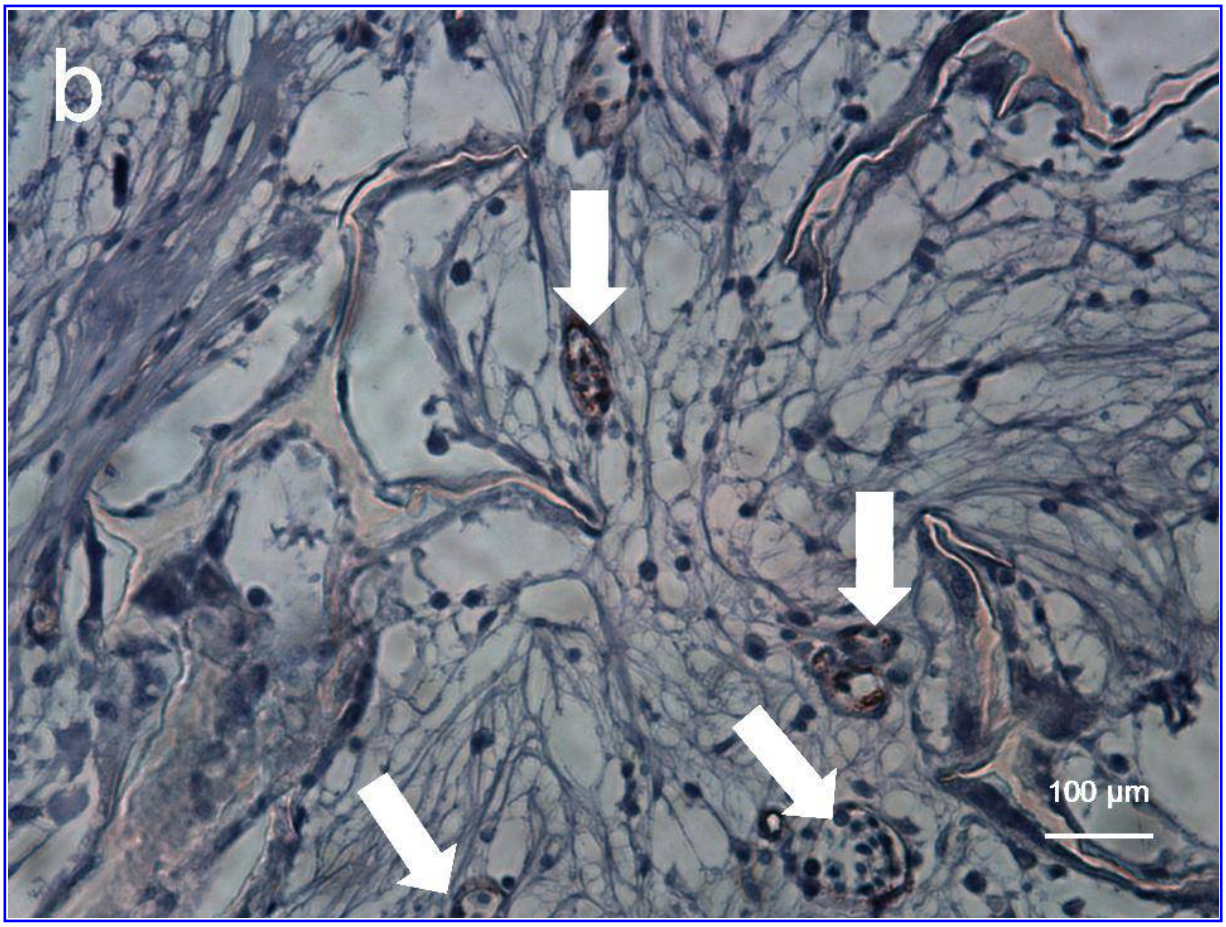

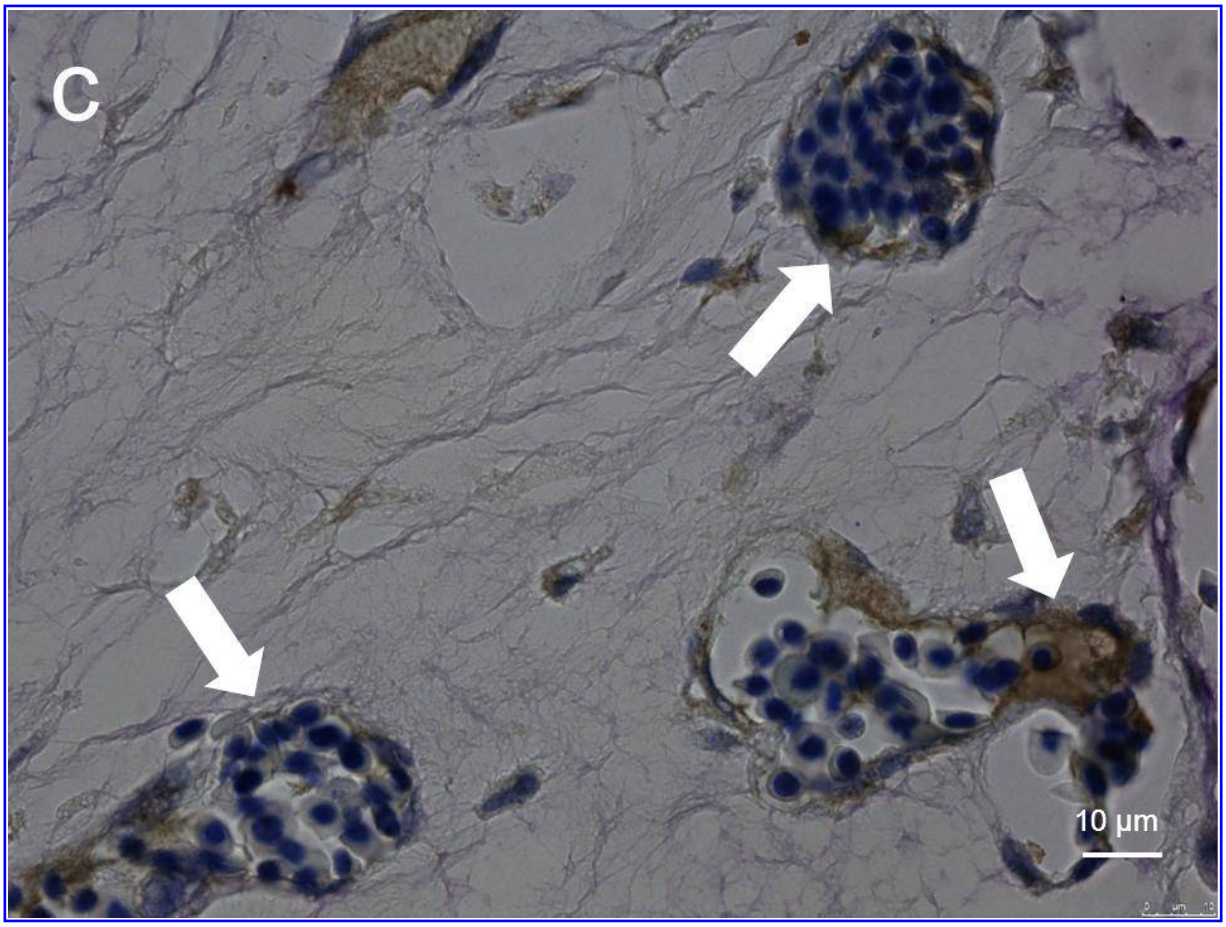

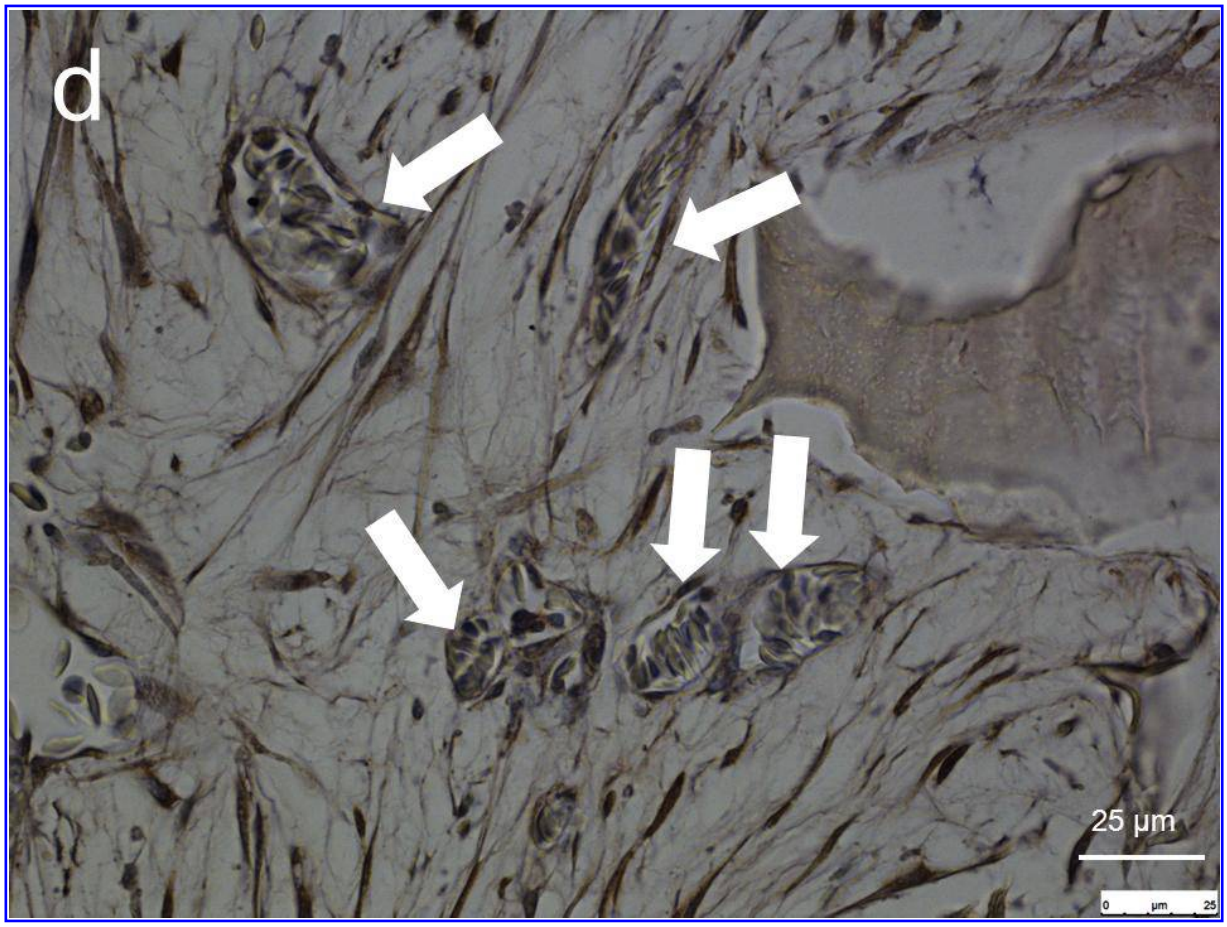

Figure 5. Histological cross sections showing the capillaries in the scaffold material: (a) H&E staining of DegraPol® at 100 x magnification; (b) immunostaining with *von Willebrand Factor* of DegraPol® at 200 x magnification; (c) immunostaining with CD31 of DegraPol® at 630 x magnification (counterstaining Toluidine Blue) and (d) immunostaining with CD31 of silk fibroin seeded with hDPSCs (counterstaining hematoxylin) at 400 x magnification. A few vessels are exemplarily highlighted by arrows.

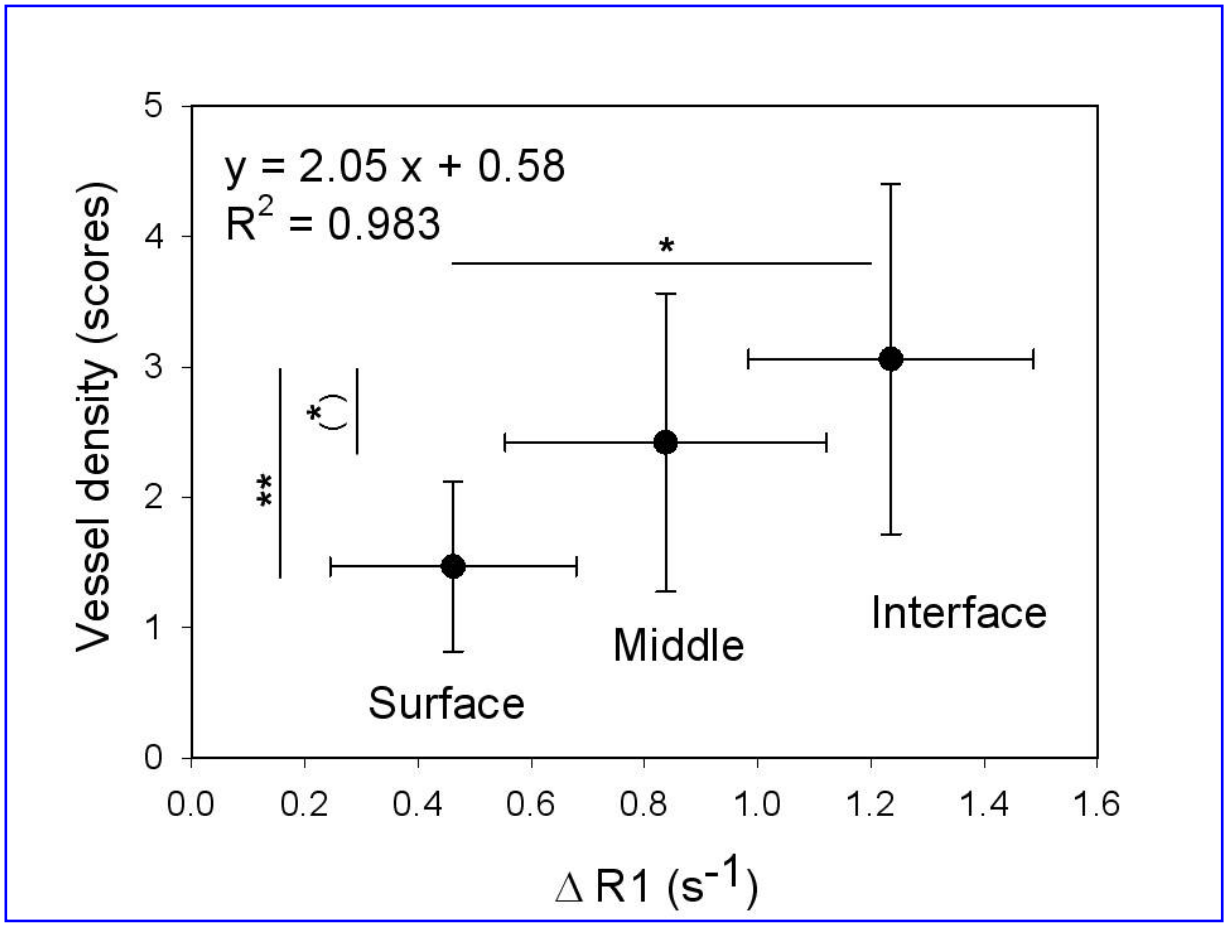

Figure 6. Relaxation rate change ΔR_1 as a measure of perfusion capacity versus vessel density obtained by semi-quantitative scoring of histological slices in three regions of interest at the interface, middle and surface of the scaffold-CAM complex. Relaxation rate change and vessel density in the scaffold are highest at the interface to the CAM and decrease with distance from the CAM. Scores **1** = < 10, **1.5**= 10 - 30, **2** = 30 - 50, **2.5** = 50 - 70, **3** = 70 - 90, **3.5** = 90 - 110, **4** = 110 – 130, **4.5** = 130 - 150 and **5** = > 150 vessels counted in a cross-section of 32 mm^2. Values are given as means ± standard deviation. *P*-values are denoted as (*) is $p < 0.1$; * $p < 0.05$ and ** $p < 0.01$.

Supplementary Information Figure 1. Typical images of H&E stained sections showing examples of scoring levels with a range from 1 to 5: **1** = < 10, **2** = 30 - 50, **3** = 70 - 90, **4** = 110 - 130 and **5** = > 150 vessels counted in a cross-section of 32 mm^2.

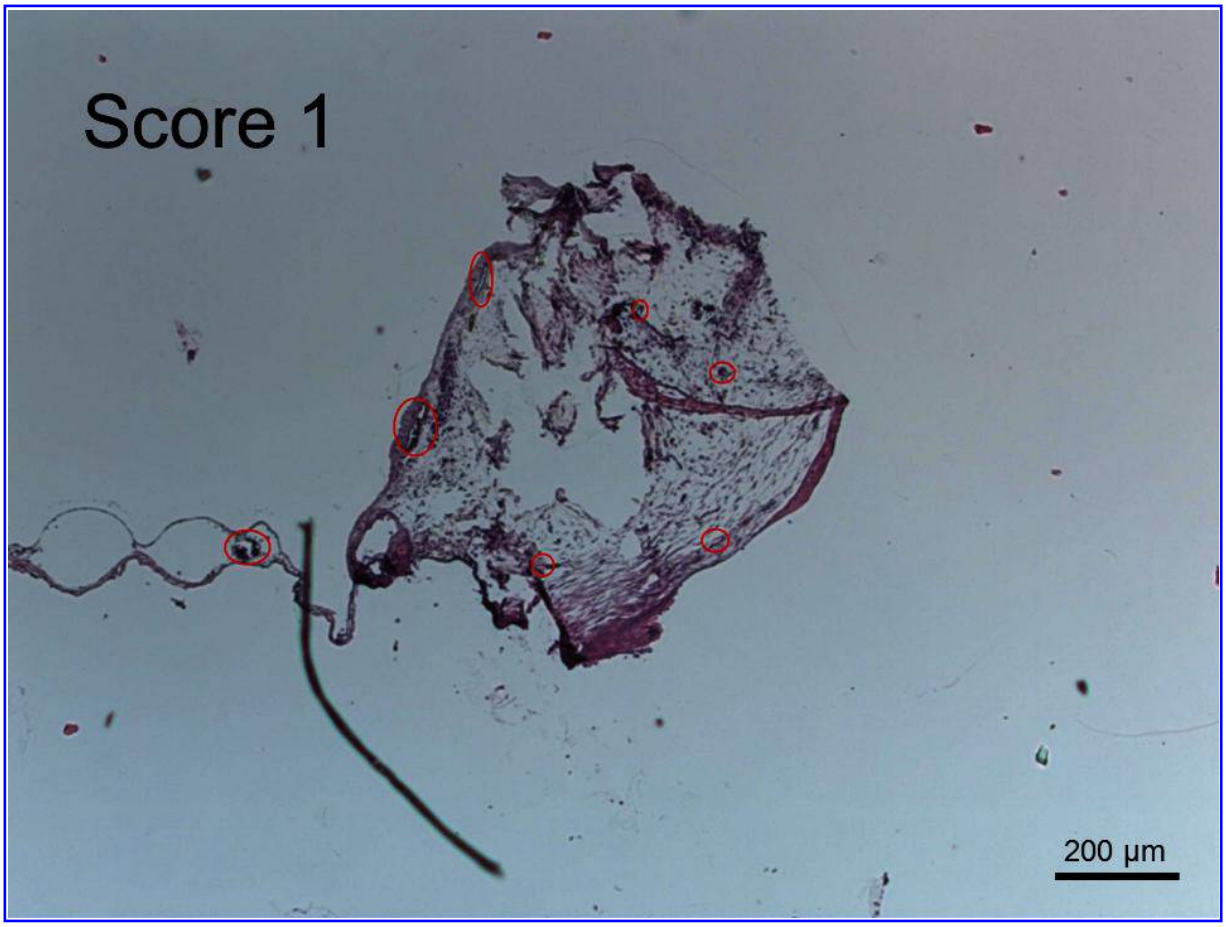

Supplementary Information Figure 1. Typical images of H&E stained sections showing examples of scoring levels with a range from 1 to 5: 1 = < 10, 2 = 30 - 50, 3 = 70 - 90, 4 = 110 - 130 and 5 = > 150 vessels counted in a cross-section of 32 mm2.

Supplementary Information Figure 1. Typical images of H&E stained sections showing examples of scoring levels with a range from 1 to 5: 1 = < 10, 2 = 30 - 50, 3 = 70 - 90, 4 = 110 - 130 and 5 = > 150 vessels counted in a cross-section of 32 mm2.

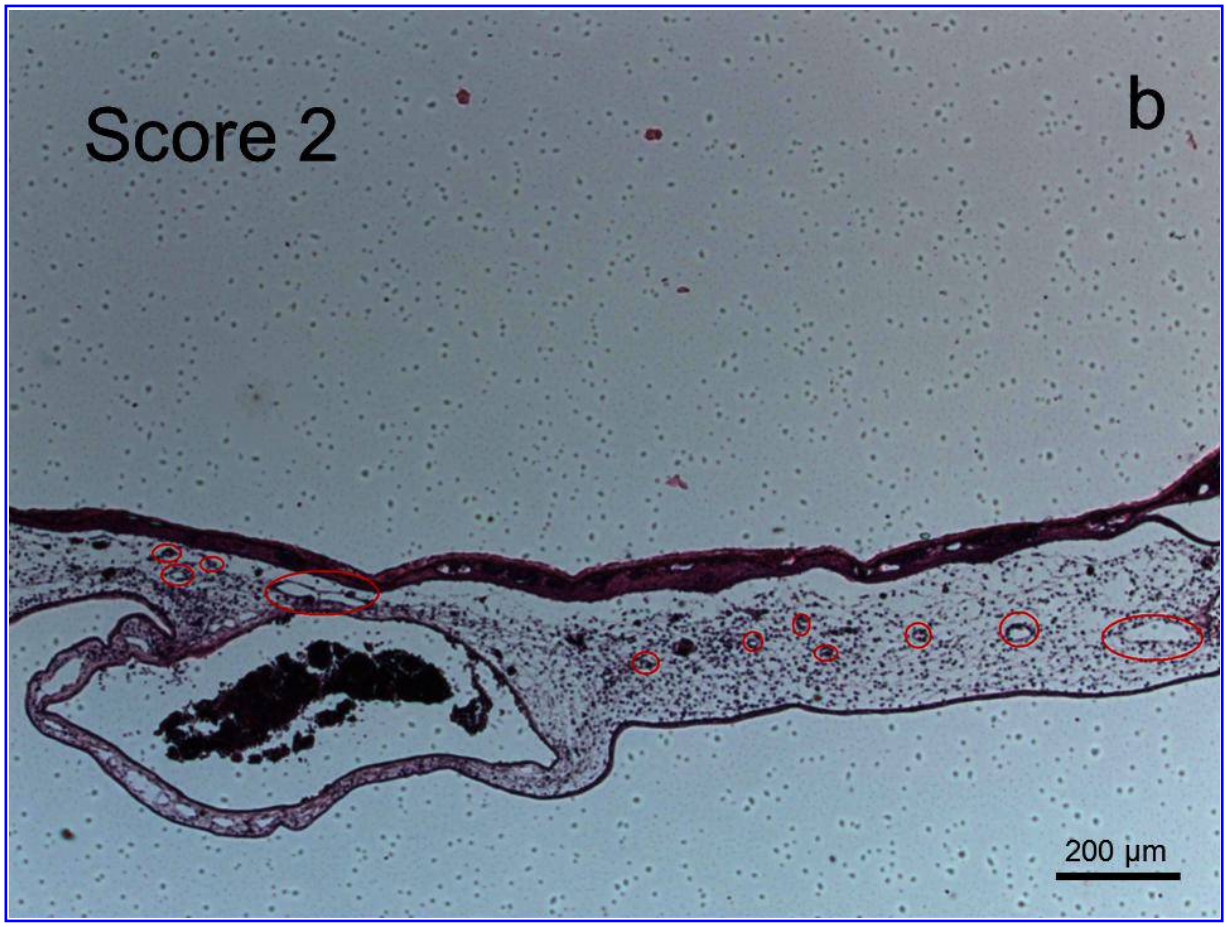

Supplementary Information Figure 1. Typical images of H&E stained sections showing examples of scoring levels with a range from 1 to 5: 1 = < 10, 2 = 30 - 50, 3 = 70 - 90, 4 = 110 - 130 and 5 = > 150 vessels counted in a cross-section of 32 mm2.

Supplementary Information Figure 1. Typical images of H&E stained sections showing examples of scoring levels with a range from 1 to 5: 1 = < 10, 2 = 30 - 50, 3 = 70 - 90, 4 = 110 - 130 and 5 = > 150 vessels counted in a cross-section of 32 mm2.

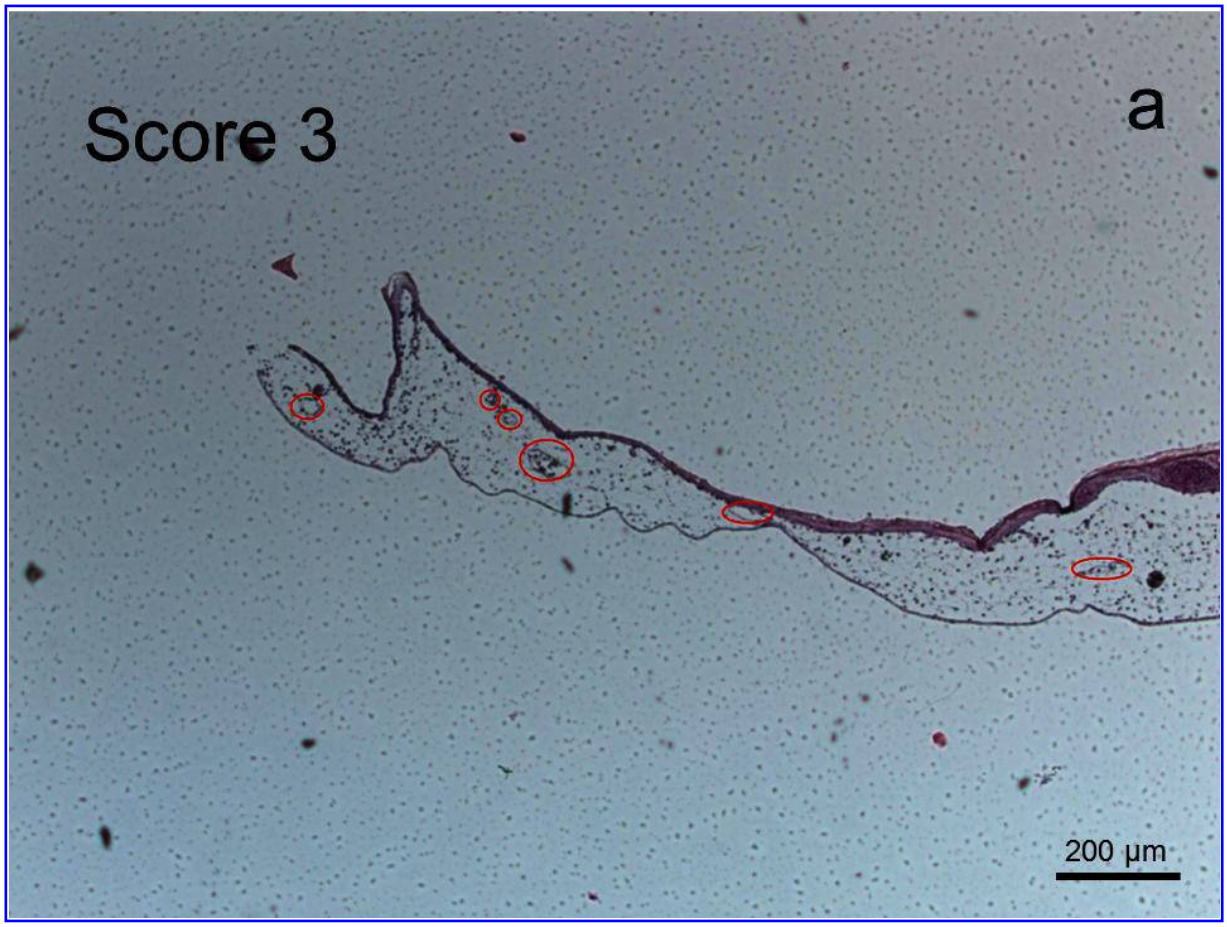

Supplementary Information Figure 1. Typical images of H&E stained sections showing examples of scoring levels with a range from 1 to 5: 1 = < 10, 2 = 30 - 50, 3 = 70 - 90, 4 = 110 - 130 and 5 = > 150 vessels counted in a cross-section of 32 mm2.

Supplementary Information Figure 1. Typical images of H&E stained sections showing examples of scoring levels with a range from 1 to 5: 1 = < 10, 2 = 30 - 50, 3 = 70 - 90, 4 = 110 - 130 and 5 = > 150 vessels counted in a cross-section of 32 mm2.

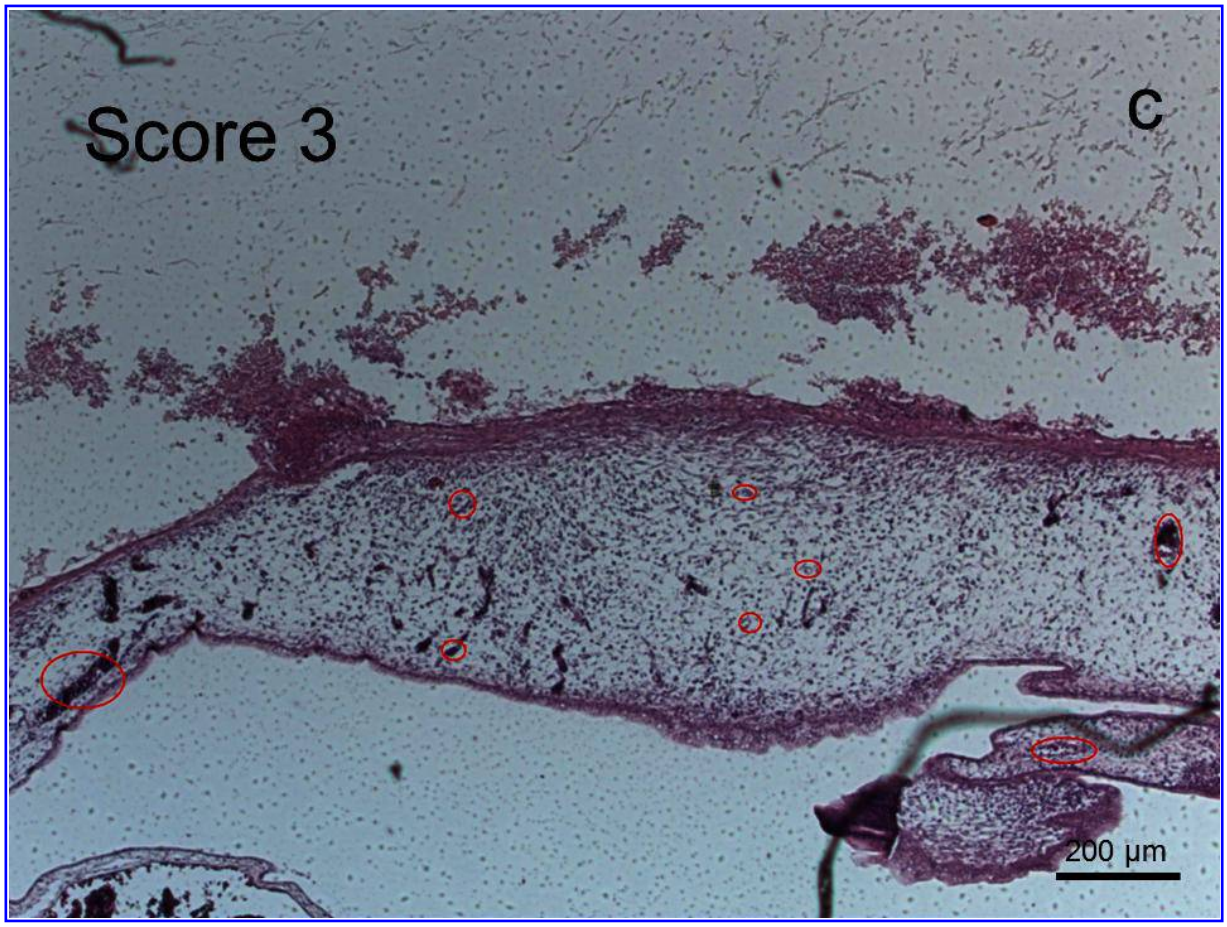

Supplementary Information Figure 1. Typical images of H&E stained sections showing examples of scoring levels with a range from 1 to 5: 1 = < 10, 2 = 30 - 50, 3 = 70 - 90, 4 = 110 - 130 and 5 = > 150 vessels counted in a cross-section of 32 mm2.

Supplementary Information Figure 1. Typical images of H&E stained sections showing examples of scoring levels with a range from 1 to 5: 1 = < 10, 2 = 30 - 50, 3 = 70 - 90, 4 = 110 - 130 and 5 = > 150 vessels counted in a cross-section of 32 mm2.

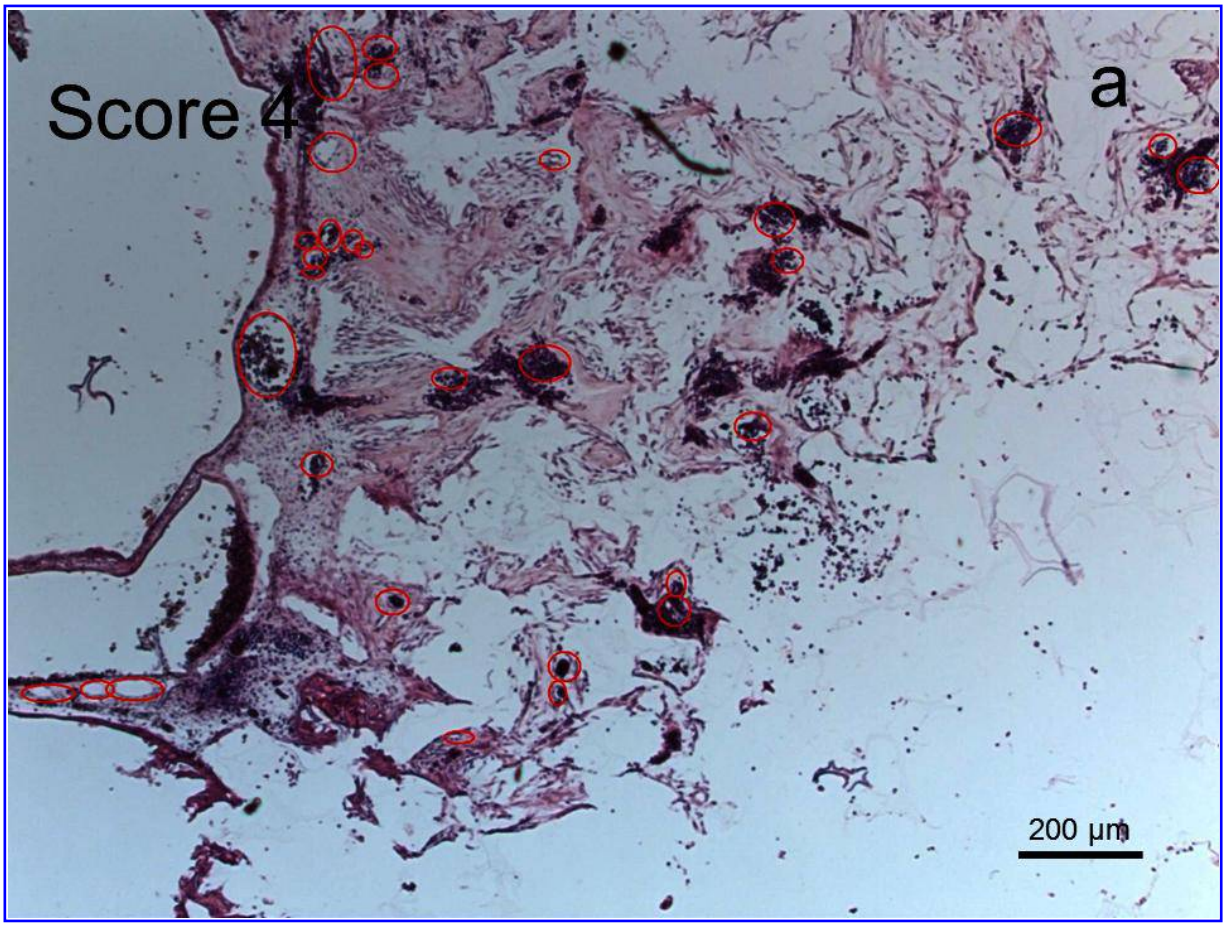

Supplementary Information Figure 1. Typical images of H&E stained sections showing examples of scoring levels with a range from 1 to 5: 1 = < 10, 2 = 30 - 50, 3 = 70 - 90, 4 = 110 - 130 and 5 = > 150 vessels counted in a cross-section of 32 mm2.

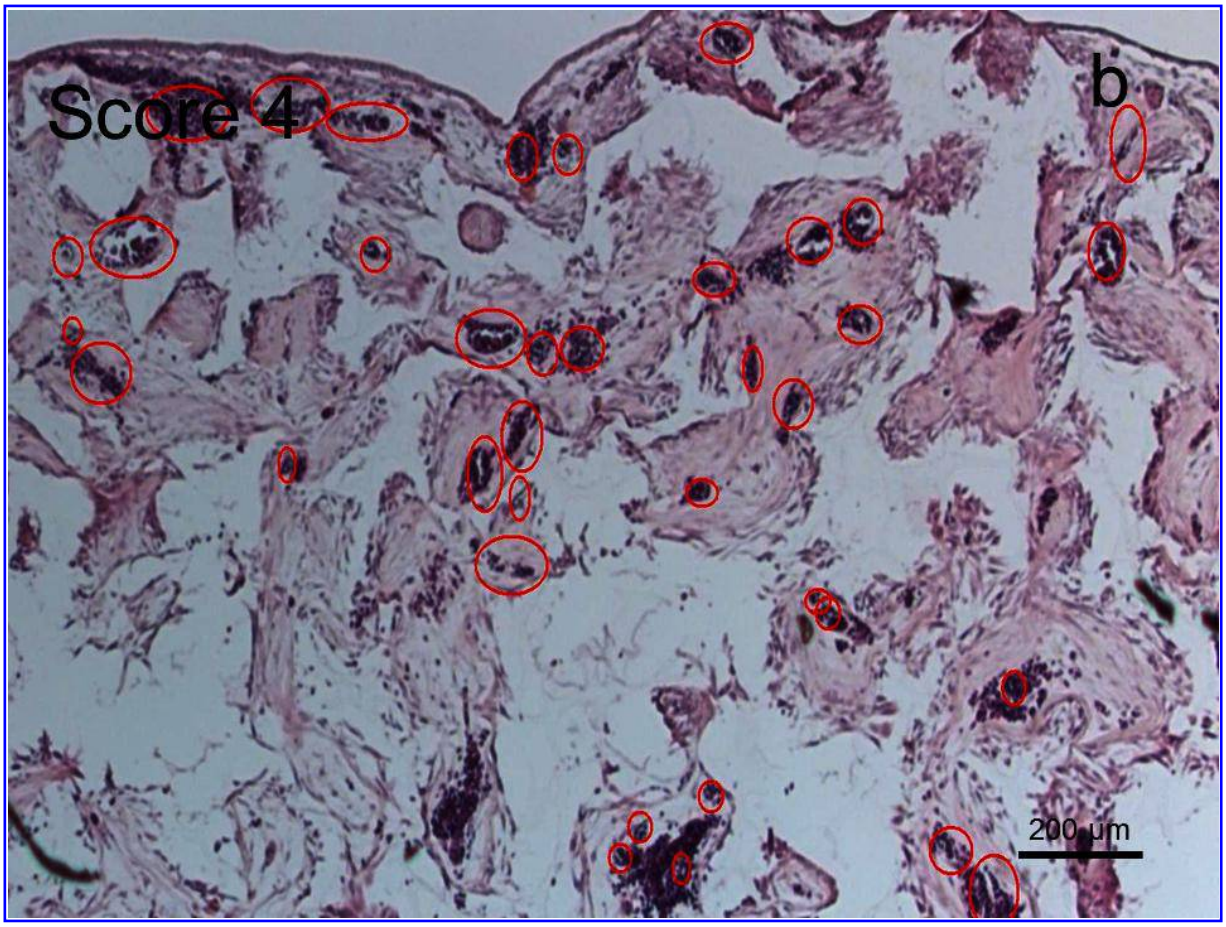

Supplementary Information Figure 1. Typical images of H&E stained sections showing examples of scoring levels with a range from 1 to 5: 1 = < 10, 2 = 30 - 50, 3 = 70 - 90, 4 = 110 - 130 and 5 = > 150 vessels counted in a cross-section of 32 mm2.

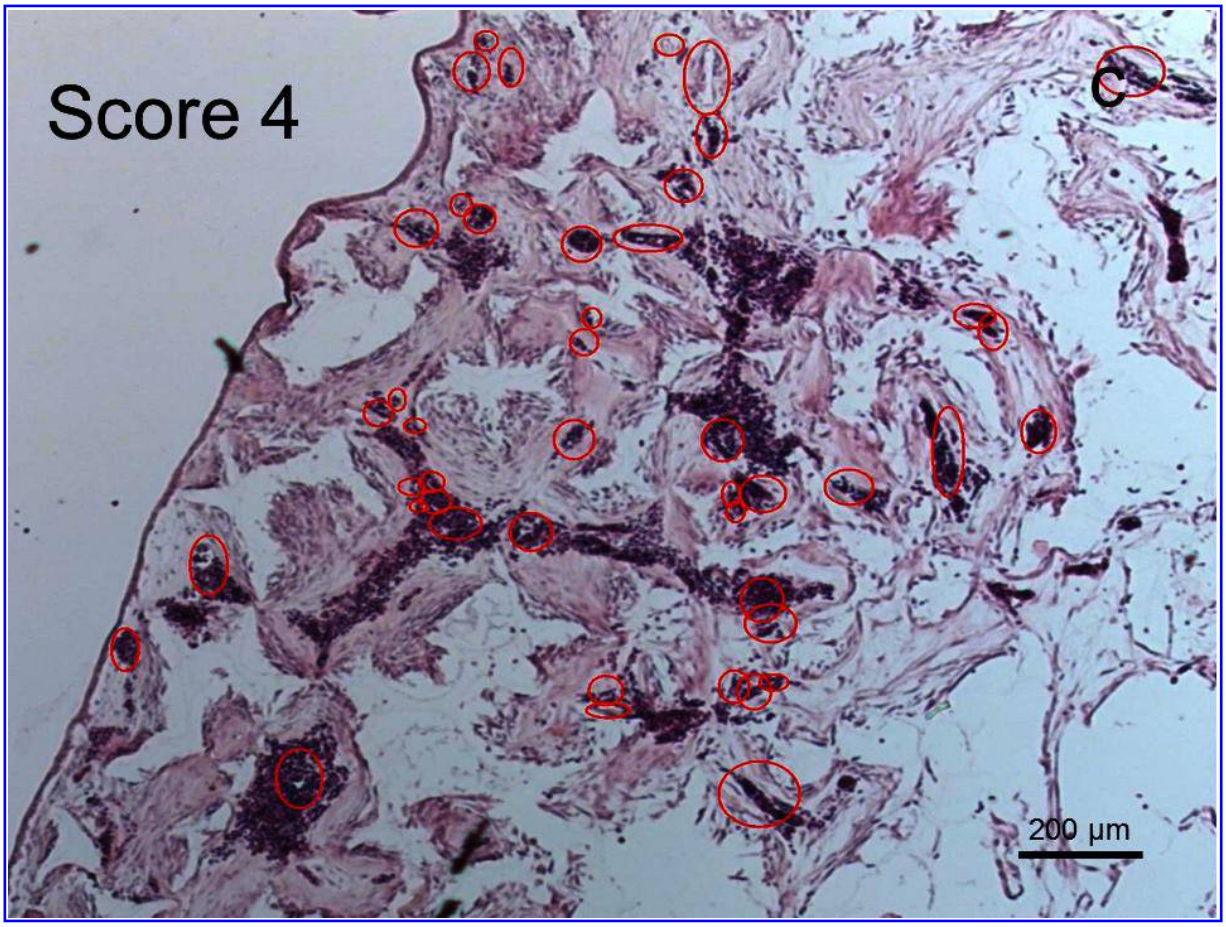

Supplementary Information Figure 1. Typical images of H&E stained sections showing examples of scoring levels with a range from 1 to 5: 1 = < 10, 2 = 30 - 50, 3 = 70 - 90, 4 = 110 - 130 and 5 = > 150 vessels counted in a cross-section of 32 mm2.

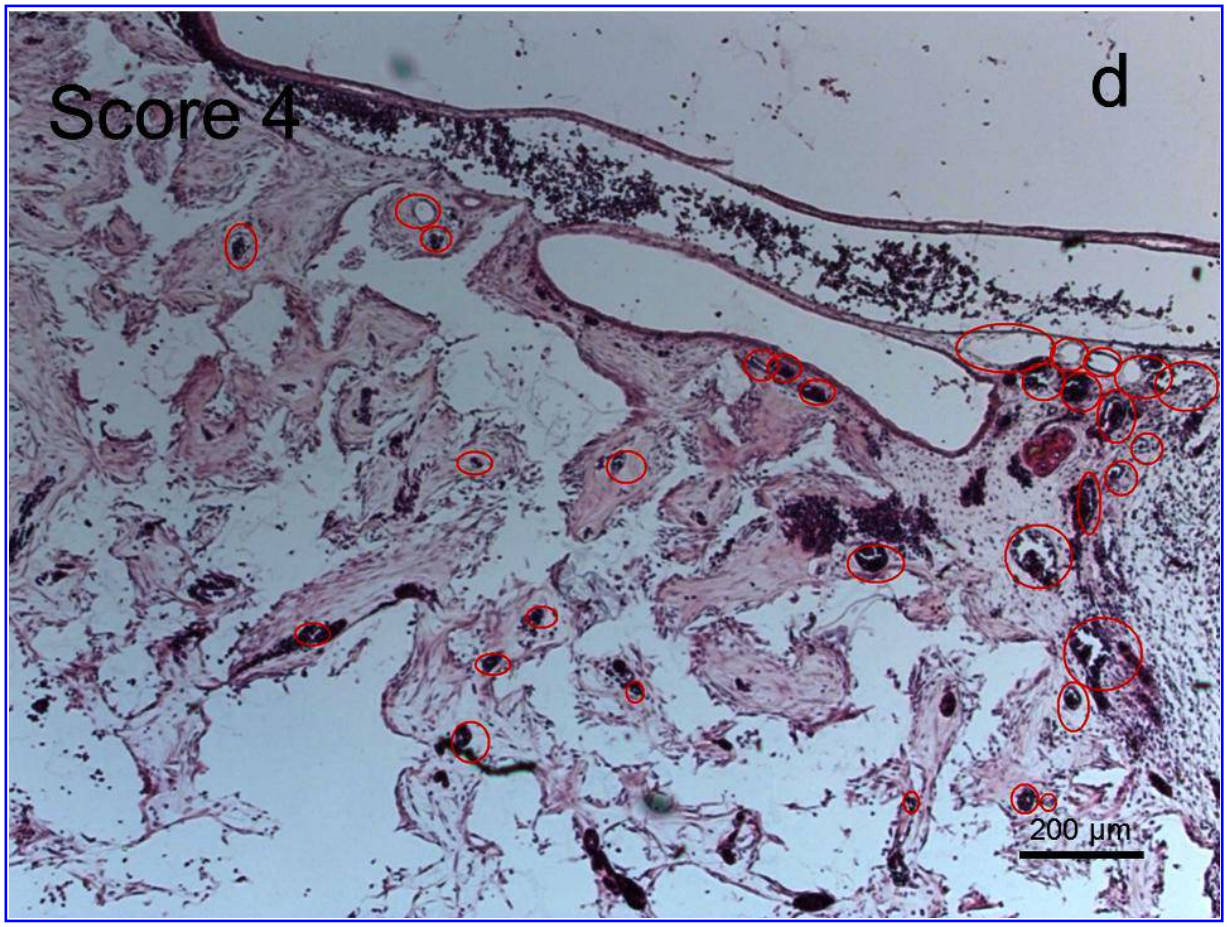

Supplementary Information Figure 1. Typical images of H&E stained sections showing examples of scoring levels with a range from 1 to 5: 1 = < 10, 2 = 30 - 50, 3 = 70 - 90, 4 = 110 - 130 and 5 = > 150 vessels counted in a cross-section of 32 mm2.

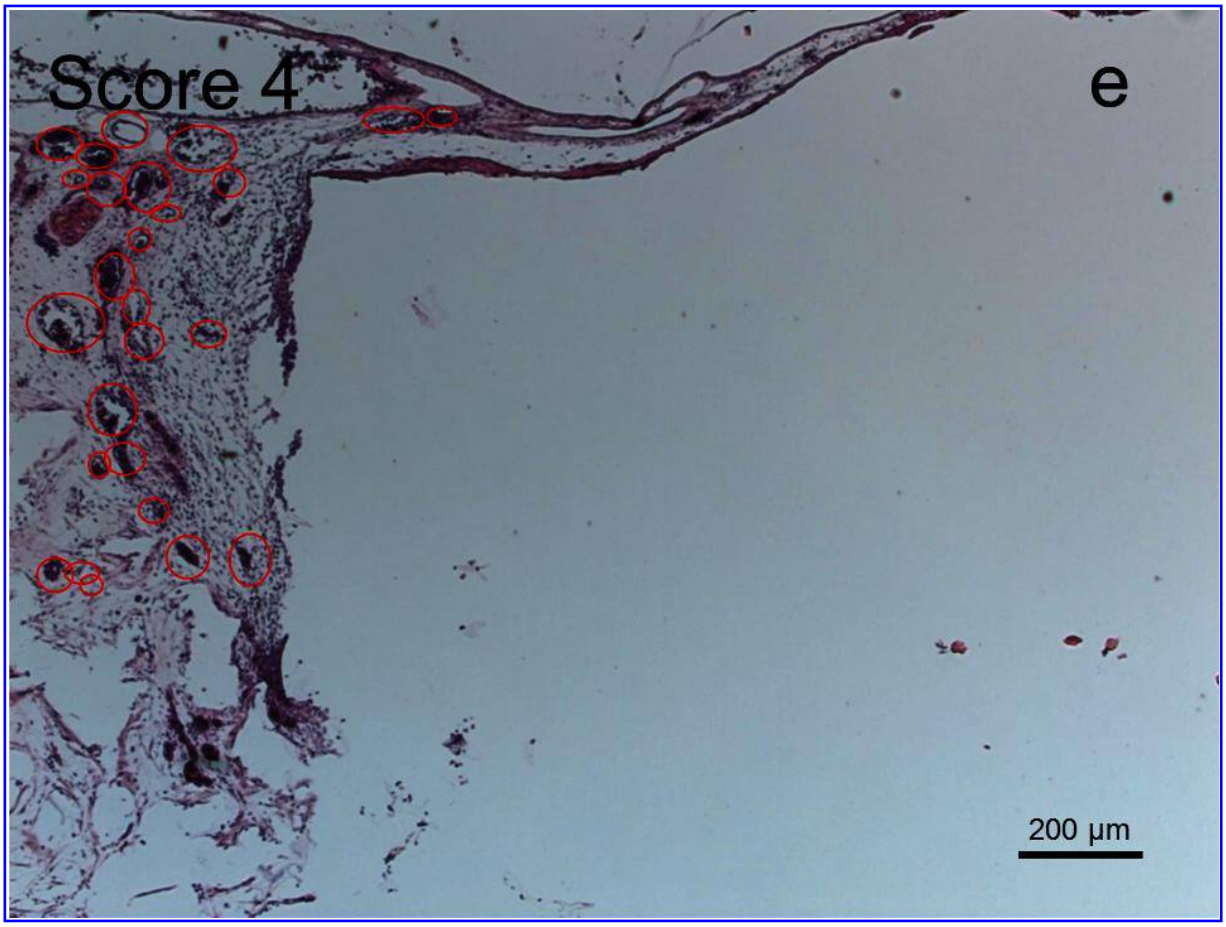

Supplementary Information Figure 1. Typical images of H&E stained sections showing examples of scoring levels with a range from 1 to 5: 1 = < 10, 2 = 30 - 50, 3 = 70 - 90, 4 = 110 - 130 and 5 = > 150 vessels counted in a cross-section of 32 mm2.

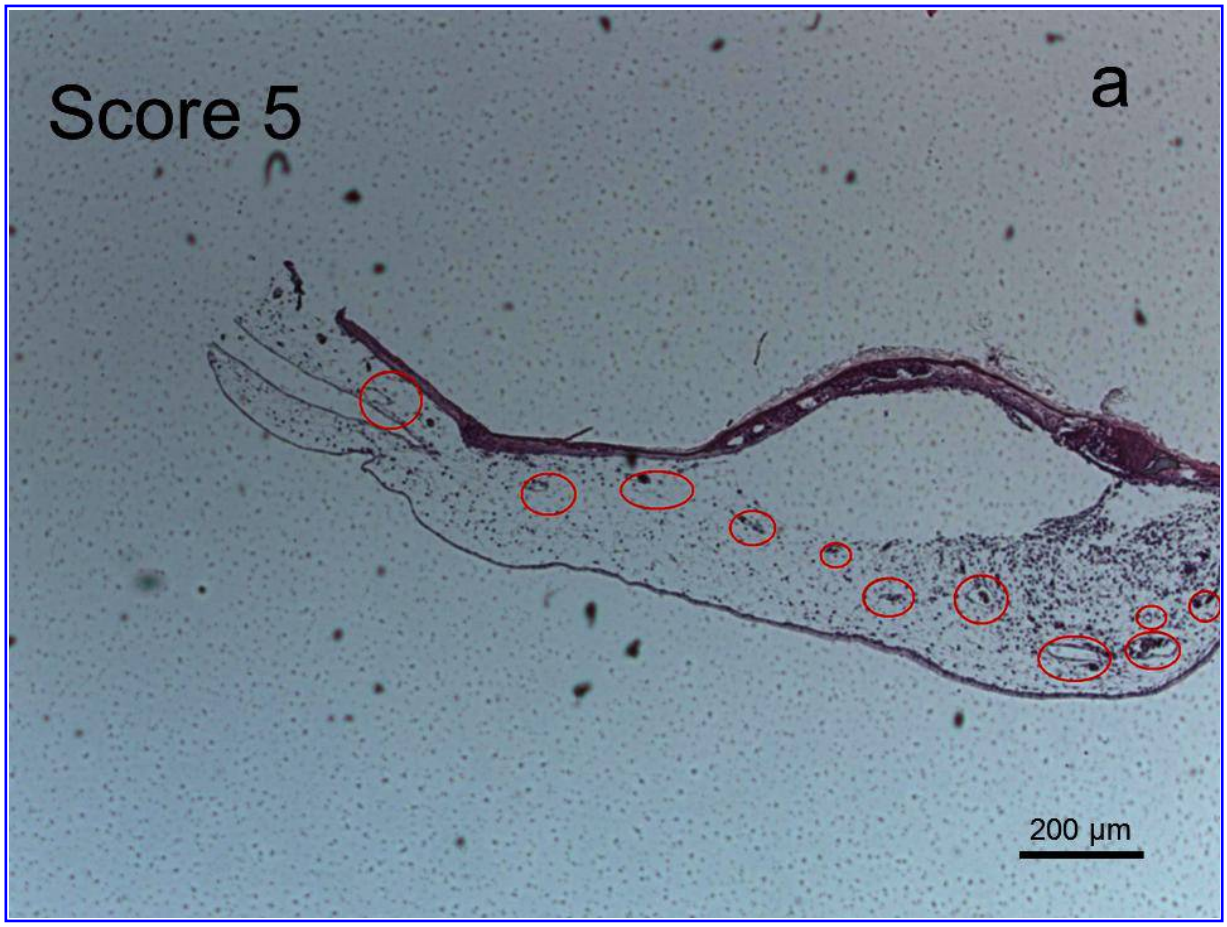

Supplementary Information Figure 1. Typical images of H&E stained sections showing examples of scoring levels with a range from 1 to 5: 1 = < 10, 2 = 30 - 50, 3 = 70 - 90, 4 = 110 - 130 and 5 = > 150 vessels counted in a cross-section of 32 mm2.

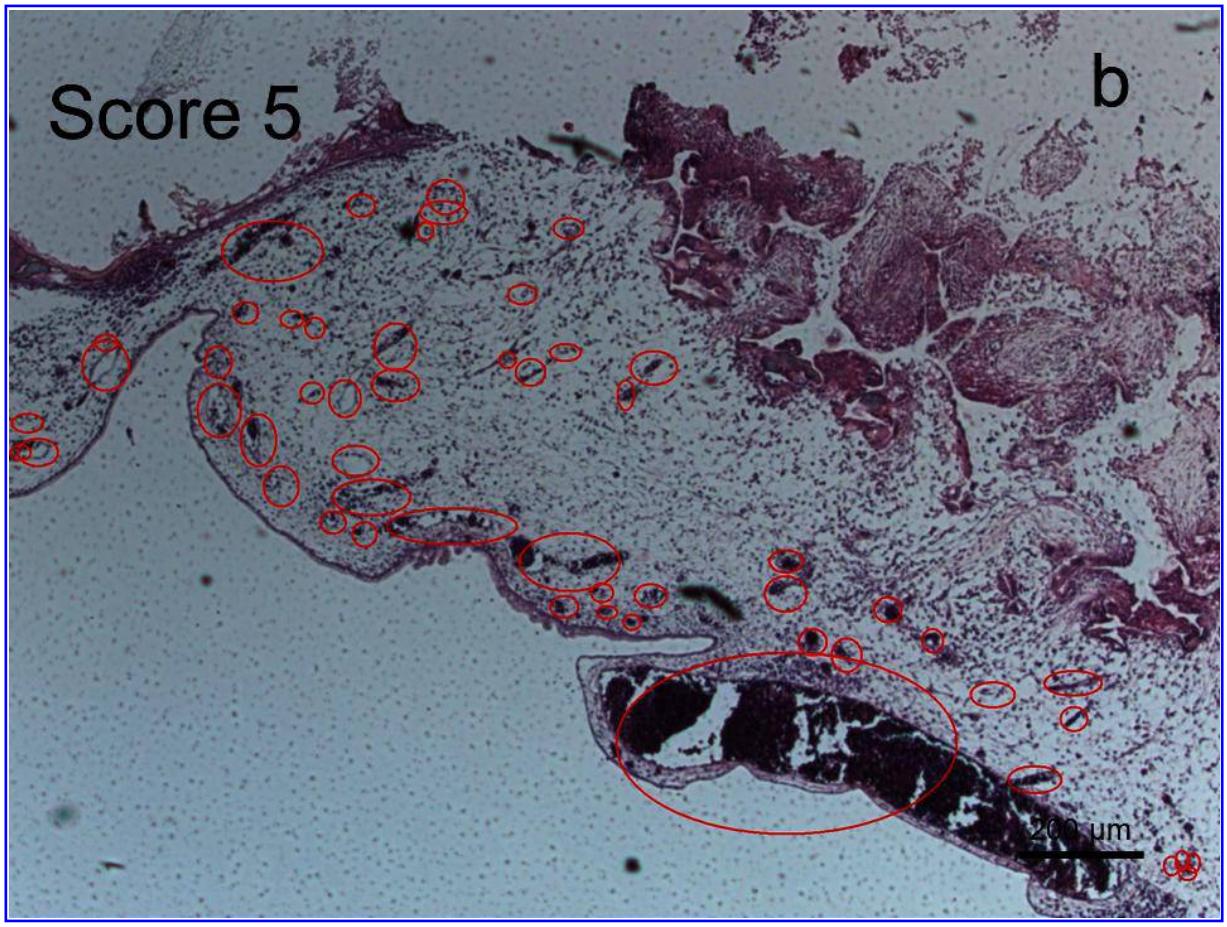

Supplementary Information Figure 1. Typical images of H&E stained sections showing examples of scoring levels with a range from 1 to 5: 1 = < 10, 2 = 30 - 50, 3 = 70 - 90, 4 = 110 - 130 and 5 = > 150 vessels counted in a cross-section of 32 mm2.

Tissue Engineering Part C: Methods

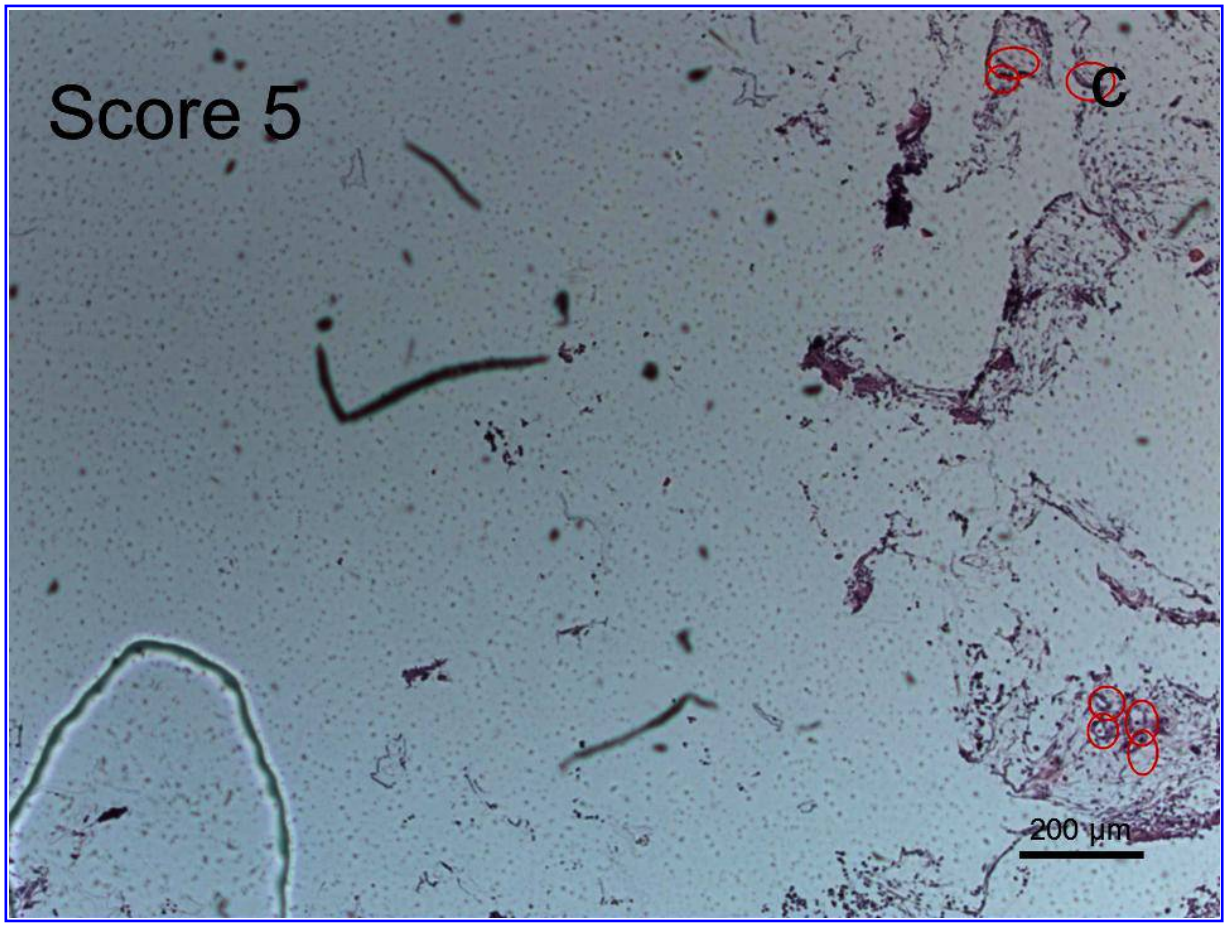

Supplementary Information Figure 1. Typical images of H&E stained sections showing examples of scoring levels with a range from 1 to 5: 1 = < 10, 2 = 30 - 50, 3 = 70 - 90, 4 = 110 - 130 and 5 = > 150 vessels counted in a cross-section of 32 mm2.

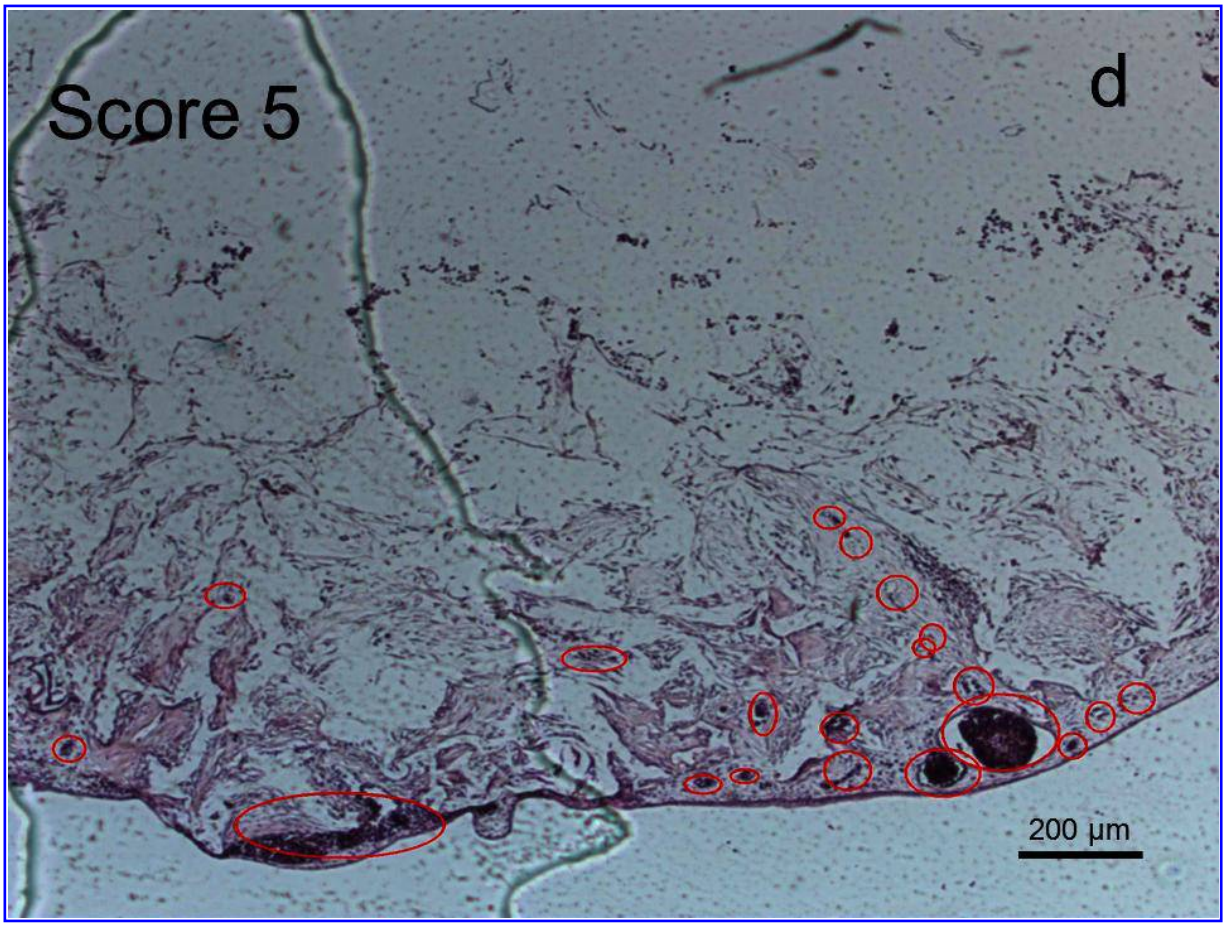

Supplementary Information Figure 1. Typical images of H&E stained sections showing examples of scoring levels with a range from 1 to 5: 1 = < 10, 2 = 30 - 50, 3 = 70 - 90, 4 = 110 - 130 and 5 = > 150 vessels counted in a cross-section of 32 mm2.

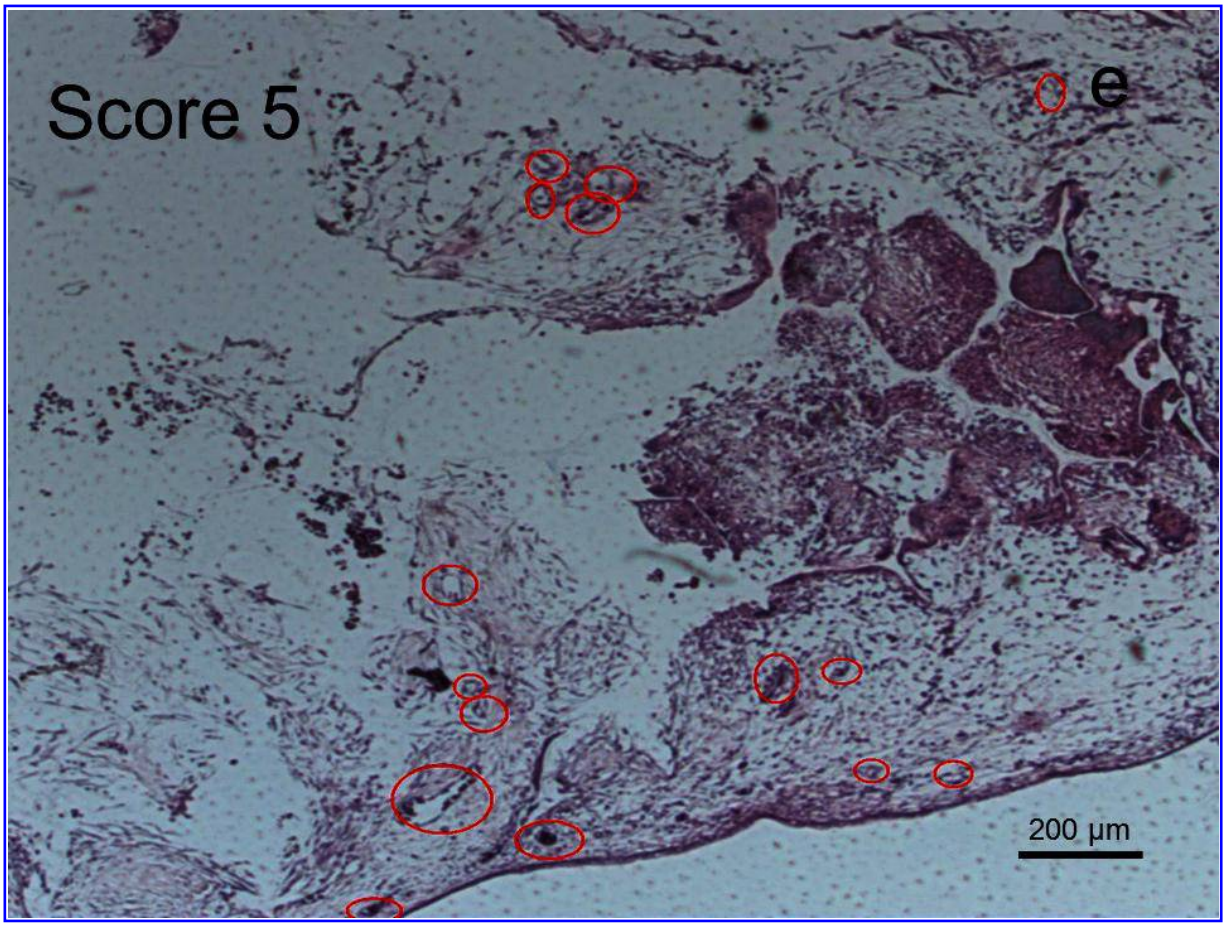

Supplementary Information Figure 1. Typical images of H&E stained sections showing examples of scoring levels with a range from 1 to 5: 1 = < 10, 2 = 30 - 50, 3 = 70 - 90, 4 = 110 - 130 and 5 = > 150 vessels counted in a cross-section of 32 mm2.

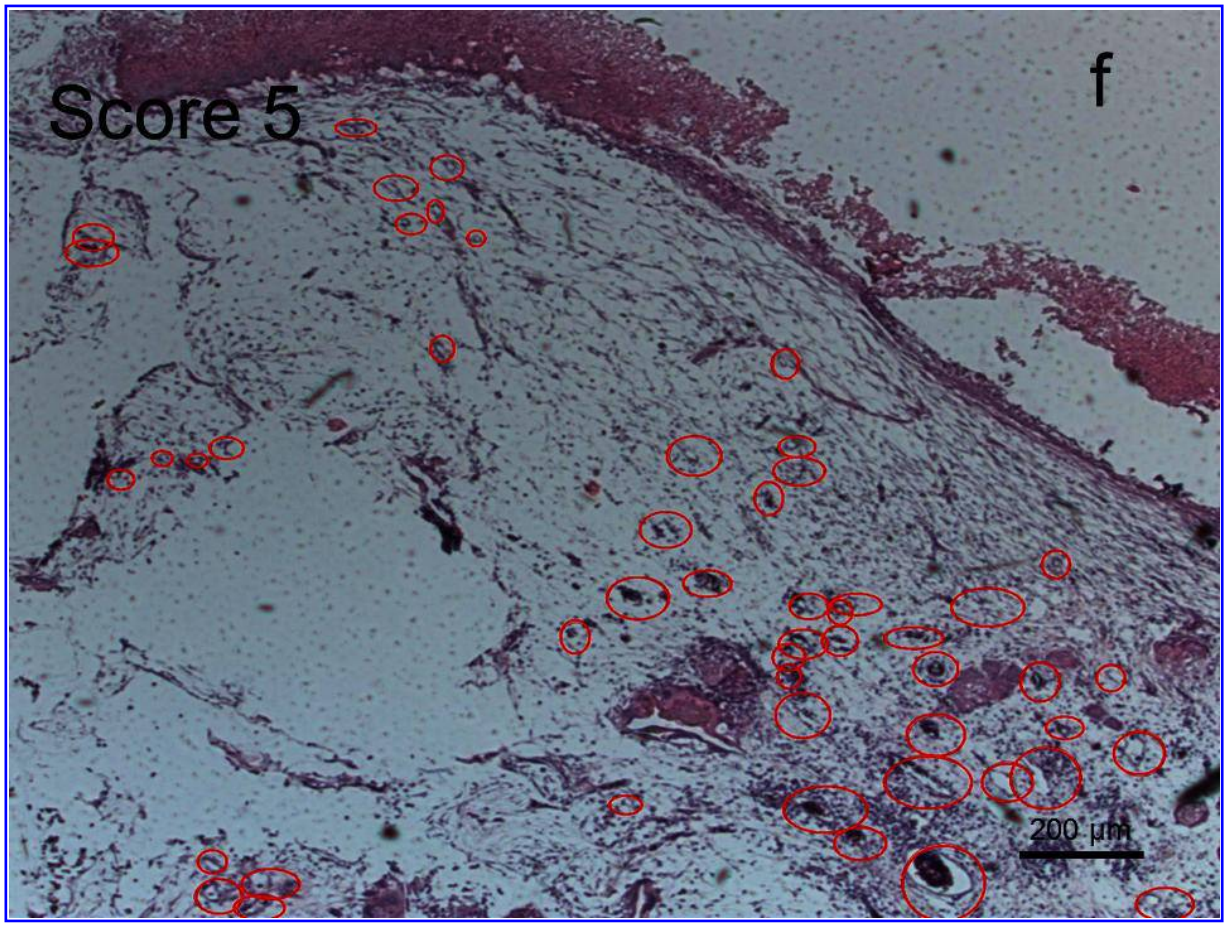

Supplementary Information Figure 1. Typical images of H&E stained sections showing examples of scoring levels with a range from 1 to 5: 1 = < 10, 2 = 30 - 50, 3 = 70 - 90, 4 = 110 - 130 and 5 = > 150 vessels counted in a cross-section of 32 mm2.

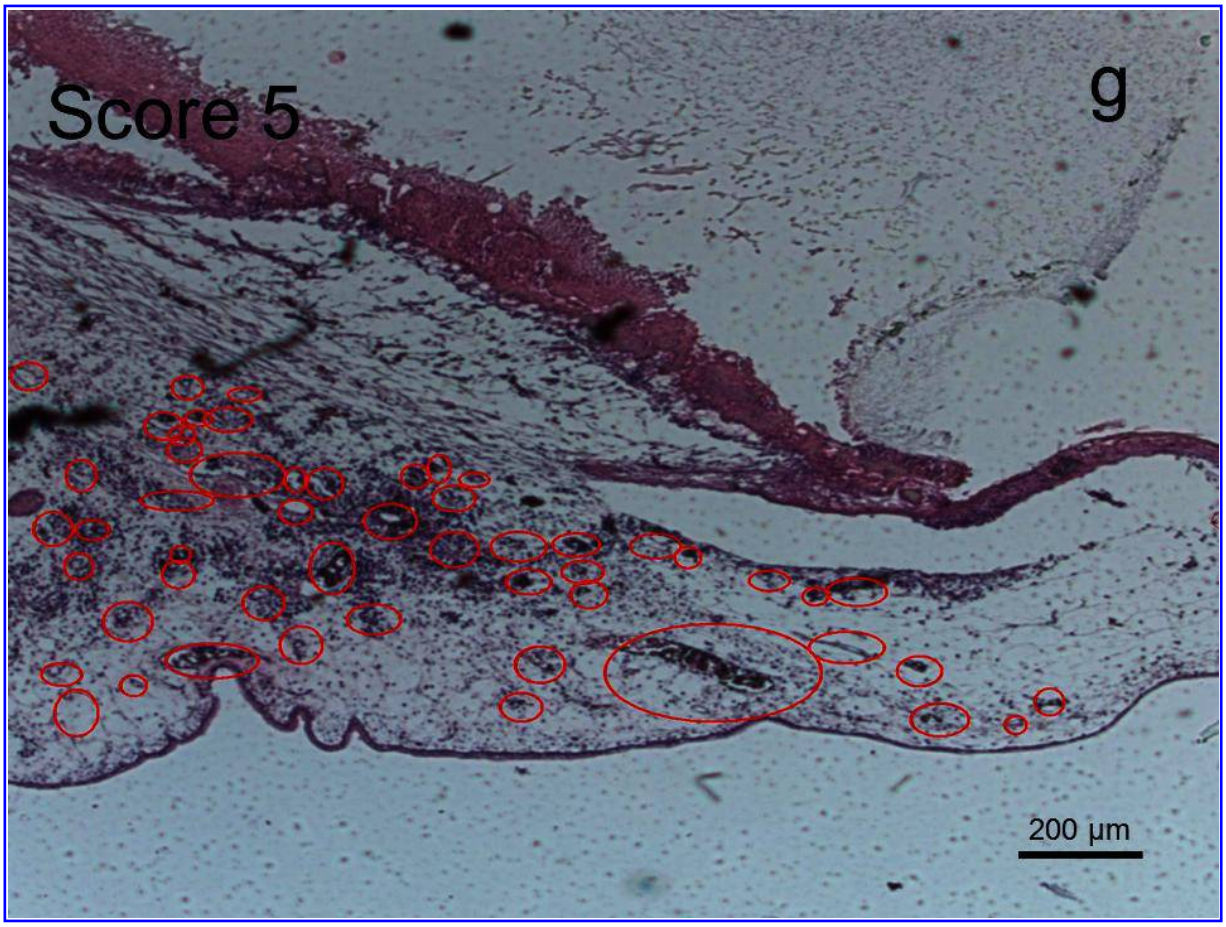

Supplementary Information Figure 1. Typical images of H&E stained sections showing examples of scoring levels with a range from 1 to 5: 1 = < 10, 2 = 30 - 50, 3 = 70 - 90, 4 = 110 - 130 and 5 = > 150 vessels counted in a cross-section of 32 mm2.

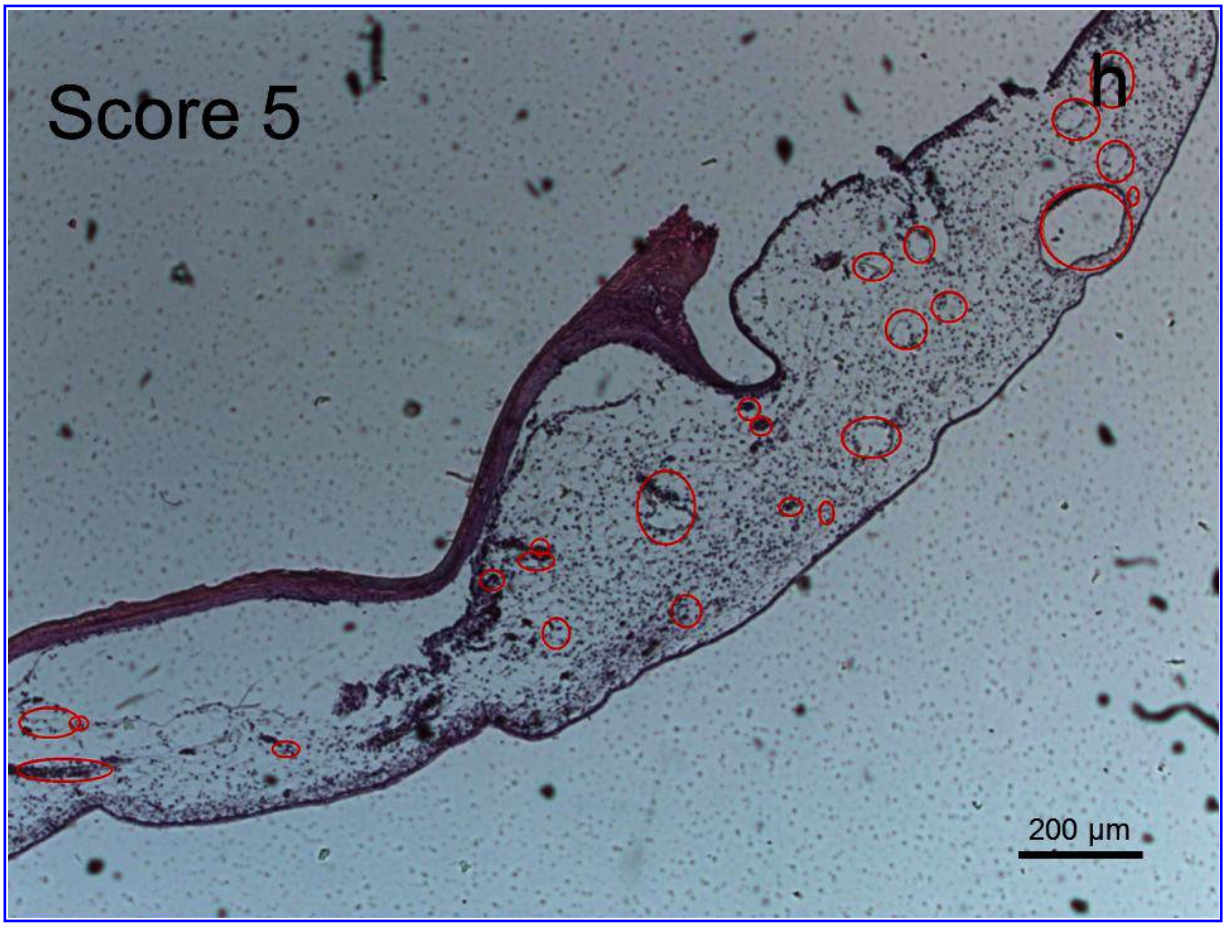

Supplementary Information Figure 1. Typical images of H&E stained sections showing examples of scoring levels with a range from 1 to 5: 1 = < 10, 2 = 30 - 50, 3 = 70 - 90, 4 = 110 - 130 and 5 = > 150 vessels counted in a cross-section of 32 mm2.